Since January 2020 Elsevier has created a COVID-19 resource centre with free information in English and Mandarin on the novel coronavirus COVID-19. The COVID-19 resource centre is hosted on Elsevier Connect, the company's public news and information website.

C5aR inhibition of nonimmune cells suppresses inflammation and maintains epithelial integrity in SARS-CoV-2–infected primary human airway epithelia

Wilfried Posch, PhD,[a]* Jonathan Vosper, PhD,[b]* Asma Noureen, PhD,[a] Viktoria Zaderer, MSc,[a] Christina Witting,[a] Giulia Bertacchi, MSc,[a] Ronald Gstir, PhD,[c] Przemyslaw A. Filipek, PhD,[c] Günther K. Bonn, PhD,[c] Lukas A. Huber, MD,[c,d] Rosa Bellmann-Weiler, MD,[e] Cornelia Lass-Flörl, MD,[a] and Doris Wilflingseder, PhD[a] *Innsbruck, Austria*

Background: Excessive inflammation triggered by a hitherto undescribed mechanism is a hallmark of severe acute respiratory syndrome coronavirus 2 (SARS-CoV-2) infections and is associated with enhanced pathogenicity and mortality.
Objective: Complement hyperactivation promotes lung injury and was observed in patients suffering from Middle East respiratory syndrome-related coronavirus, SARS-CoV-1, and SARS-CoV-2 infections. Therefore, we investigated the very first interactions of primary human airway epithelial cells on exposure to SARS-CoV-2 in terms of complement component 3 (C3)-mediated effects.
Methods: For this, we used highly differentiated primary human 3-dimensional tissue models infected with SARS-CoV-2 patient isolates. On infection, viral load, viral infectivity, intracellular complement activation, inflammatory mechanisms, and tissue destruction were analyzed by real-time RT-PCR, high content screening, plaque assays, luminex analyses, and transepithelial electrical resistance measurements.
Results: Here, we show that primary normal human bronchial and small airway epithelial cells respond to SARS-CoV-2 infection by an inflated local C3 mobilization. SARS-CoV-2 infection resulted in exaggerated intracellular complement activation and destruction of the epithelial integrity in monolayer cultures of primary human airway cells and highly differentiated, pseudostratified, mucus-producing, ciliated respiratory tissue models. SARS-CoV-2–infected 3-dimensional cultures secreted significantly higher levels of C3a and the proinflammatory cytokines IL-6, monocyte chemoattractant protein 1, IL-1α, and RANTES.
Conclusions: Crucially, we illustrate here for the first time that targeting the anaphylotoxin receptors C3a receptor and C5a receptor in nonimmune respiratory cells can prevent intrinsic lung inflammation and tissue damage. This opens up the exciting possibility in the treatment of COVID-19. (J Allergy Clin Immunol 2021;147:2083-97.)

Key words: *SARS-CoV-2, complement, anaphylatoxin receptors, primary human airway epithelial cells*

Early events occurring directly after severe acute respiratory syndrome coronavirus 2 (SARS-CoV-2) transmission to respiratory tissues can influence the outcome in the context of disease severity—in some patients, infection with coronavirus disease 19 (COVID-19) results in excessive activation of the immune response at epithelial/immune barriers and the generation of a proinflammatory milieu.[1,2] The development of a cytokine storm and acute lung injury, causing acute respiratory distress syndrome (ARDS), are potential undesirable consequences of the disease. ARDS accompanied by systemic coagulopathy are critical aspects of morbidity and mortality in COVID-19.[3,4] These overshooting immune responses triggered by incoming viruses result in extensive tissue destruction during severe cases, resulting in tissue injury and multiorgan failure.[5,6] Complement may be among the factors responsible for the immune overactivation, because complement deposition and high anaphylatoxin serum levels have been reported in patients with severe/critical disease.[7] As recently shown in transcriptome analyses of bronchoalveolar lavages of patients, the complement system was among the most significantly upregulated intracellular pathways following SARS-CoV-2 infection.[8] In addition, the transcriptomes of primary normal human bronchial epithelial cells infected *in vitro* with SARS-CoV-2 revealed an enriched complement signature.[8] Very recently, Ramlall et al[9] identified in addition to type I IFN– and IL-6–dependent inflammatory responses, a robust engagement of complement and coagulation pathways following SARS-CoV-2 infection. Here, we further analyzed local complement activation at the protein level in a highly differentiated primary human 3-dimensional (3D) respiratory model on *in vitro* infection using a SARS-CoV-2 clinical specimen.[10,11] In such

From [a]the Institute of Hygiene and Medical Microbiology, Medical University of Innsbruck; [b]the Institute of Medical Biochemistry, Medical University of Innsbruck, Innsbruck; [c]ADSI - Austrian Drug Screening Institute GmbH, Innsbruck; [d]the Institute of Cell Biology, Biocenter Innsbruck, Medical University of Innsbruck; and [e]the University Hospital of Internal Medicine II, Medical University of Innsbruck, Innsbruck.
*These authors contributed equally to this work.
The authors were supported by the Austrian Science Fund (FWF; grant no. P 34070-B to W.P. and grant no. P33510-B to D.W.), Marie Skłodowska-Curie action (CORVOS EU-H2020-MSCA-ITN-2019; grant no. 860064 to D.W.), the Anniversary Fund of the Austrian National Bank (OeNB; grant no. P 17614 to W.P. and grant no. 17633 to D.W.), and the National Institute of Allergy and Infectious Diseases (grant no. UM1AI068618 to D.W.).
Disclosure of potential conflict of interest: The authors declare that they have no relevant conflicts of interest.
Received for publication November 11, 2020; revised March 25, 2021; accepted for publication March 29, 2021.
Available online April 20, 2021.
Corresponding author: Doris Wilflingseder, PhD, or Wilfried Posch, PhD, Institute of Hygiene and Medical Microbiology, Schöpfstrasse 41/R311, 6020 Innsbruck, Austria. E-mail: doris.wilflingseder@i-med.ac.at. Or: wilfried.posch@i-med.ac.at.
The CrossMark symbol notifies online readers when updates have been made to the article such as errata or minor corrections
0091-6749

https://doi.org/10.1016/j.jaci.2021.03.038

Abbreviations used

3D: 3-Dimensional
ALI: Air-liquid interphase
ARDS: Acute respiratory distress syndrome
BF: Brightfield
C3: Complement component 3
C3aR/C5aR: C3a/C5a receptor, anaphylatoxin receptors
COVID-19: Coronavirus disease 2019
CPE: Cytopathic effect
dpi: Day postinfection
HAE: Human airway epithelia
IC: Intracellular
MAC: Membrane attack complex
MCP-1: Monocyte chemotactic protein 1
MOI: Multiplicity of infection
PFU: Plaque-forming unit
SARS-CoV-2: Severe acute respiratory syndrome coronavirus 2
TCC: Terminal complement complex
TEER: Transepithelial electrical resistance
UI: Uninfected

cultures, complete destruction of epithelial integrity was observed on viral infection and was associated with exacerbated complement component 3 (C3) production, membrane attack complex (MAC) formation as well as detachment of cells and release of virus into the supernatants. Virus infection was detected not only in outermost layers but virus particles were seen to penetrate deeply into the pseudostratified epithelium as well, with a concomitant C3 activation or probably also deposition on dead or damaged cells being observed in these layers. Besides C3 activation, significantly higher levels of C3a desArg, tissue damage, and proinflammatory cytokines, such as IL-6, monocyte chemotactic protein 1 (MCP-1), IL-1α, and RANTES, were detected in SARS-CoV-2–infected tissue models. Although C3aR blocking alleviated viral infection and reduced the inflammatory response in airways, C5aR antagonism completely restored tissue integrity, significantly downmodulated local complement production, and associated therewith returned C3a and proinflammatory levels back to normal. C5aR antagonism was also shown to correlate with low viral loads. Our results point toward a novel therapeutic intervention strategy whereby complement inhibitors are administered to high-risk patients during an early stage of disease progression to prevent an excessive inflammatory response and its associated pathological consequences.

METHODS

Ethics statement

Written informed consent was obtained from all donors of leftover nasopharyngeal/oropharyngeal specimens and EDTA blood by the participating clinics. The Ethics Committee of the Medical University of Innsbruck (a copy is attached to the proposal, ECS1166/2020) approved the use of anonymized leftover specimens of patients with COVID-19 for scientific purposes.

Cell culture of tissue models

Human airway epithelia. Normal human bronchial epithelial (cat# CC-2540S) and small airway epithelial (cat# CC-2547S) cells are available in our laboratory and routinely cultured in air-liquid interface (ALI) as described.[10,11] Briefly, cells were cultured in a T75 flask for 2 to 4 days until they reached 80% confluence. The cells were trypsinized and seeded onto GrowDexT (UPM)-coated 0.33-cm^2 porous (0.4-μm) polyester membrane inserts with a seeding density of 1×10^5 cells per Transwell (Costar, Corning, New York, NY). The cells were grown to near confluence in submerged culture for 2 to 3 days in specific epithelial cell growth medium according to the manufacturer's instructions. Cultures were maintained in a humidified atmosphere with 5% CO_2 at 37°C and then transferred to ALI culture. The epithelium was expanded and differentiated using airway media from Stemcell (Germany). The number of days in development was designated relative to initiation of ALI culture, corresponding to day 0. In addition, for real-time RT-PCR analyses of uninfected (UI) and SARS-CoV-2–infected 3D tissues and supernatants, apical-out lung organoids were generated. Briefly, cryopreserved lung organoids derived from human normal lung tissue (left superior lobe) were acquired from Hubrecht Organoid Technology (HUB), Utrecht, The Netherlands (HUB-07-A2-051). These organoids were cultured according to the previously described protocol.[12,13] Because the SARS-CoV-2 receptor angiotensin-converting enzyme 2 is predominantly expressed on the apical side of the airway epithelium,[14] apical-out lung organoids were generated as recently described to expose the apical side of the lung organoids to facilitate viral infection. Apical-out organoids were further differentiated into multiciliated cells by using differentiation medium as previously reported by Zhou et al.[15]

Vero/TMPRSS2. VeroE6/TMPRSS2 is an engineered VeroE6 cell line expressing high levels of TMPRSS2 and is highly susceptible to SARS-CoV-2 infection and is used to expand SARS-CoV-2 viruses from repositories as well as patient isolates. The cell line was obtained via the Center for AIDS Reagents (National Institute for Biological Standards and Control) and is described in Matsuyama et al.[16]

Transepithelial electrical resistance measurement

Transepithelial electrical resistance (TEER) values were measured using EVOM volt-ohm-meter with STX-2 chopstick electrodes (World Precision Instruments, Stevenage, UK). Measurements on cells in ALI culture infected or not with SARS-CoV-2 plus/minus antagonists (1 μM) or treated with recombinant C5a (1 μg/mL) were taken immediately before the medium was exchanged. For measurements, 0.1 mL and 0.7 mL of medium was added to the apical and basolateral chambers, respectively. Cells were allowed to equilibrate before TEER was measured. TEER values reported were corrected for the resistance and surface area of the Transwell filters.

Staining and high content screening

To visualize SARS-CoV-2 infection in monolayers and 3D tissue models, cells were infected with clinical specimen of SARS-CoV-2 and analyzed for characteristic markers on days 2 and 5 postinfection (2 dpi and 5 dpi). For inhibition of C3aR (SB 290157, Calbiochem) and C5aR (mix of W-54011 and DF2593, 1:1, Calbiochem), commercially available antagonists were obtained from Sigma-Aldrich (St Louis, Mo). Tissue cultures were treated 2 hours before infection with 1 μM C3aR- and C5aR antagonists at the basolateral site. After infection, cells and 3D-cell cultures were fixed with 4% paraformaldehyde. Intracellular staining was performed using 1× Intracellular Staining Permeabilization Wash Buffer (10×; BioLegend, San Diego, Calif). Antibodies to detect cilia (acetylated tubulin-Alexa488, Cell Signaling Technologies, Danvers, Mass, or wheat germ agglutinin-680, Thermofisher Scientific, Waltham, Mass), mucus (Muc5AC-Alexa647, Cell Signaling Technologies), nuclei (Hoechst 33342, Cell Signaling Technologies), actin (phalloidin-Alexa647, Cell Signaling Technologies), and complement C3 (C3-FITC, Agilent Technologies, Santa Clara, Calif) were used. To investigate terminal complement complex (TCC) formation, the anti–C5b-9 (aE11 clone, Abcam, Cambridge, UK) antibody recognizing a neoepitope exposed on polymerized C9 when incorporated in the human TCC was used. Neoantigens were shown to be expressed in both MAC and fluid phase (SC5-9) complex.[17] Intracellular SARS-CoV-2 was detected using Alexa594-labeled SARS-CoV-2 antibodies against S1 and N (both Sino Biological, Beijing, China). The Alexa594-labeling kit was purchased from Abcam. Cells and 3D cultures were thoroughly washed following the staining procedure using the permeabilization

buffer, sterile-filtered D-PBS, and finally mounted in Mowiol. To study these complex models using primary cells cultured in 3D and to generate detailed phenotypic fingerprints for deeper biological insights in a high-throughput manner, the Operetta CLS System (PerkinElmer, Waltham, Mass) was applied. Spot analyses, nanotube evaluation, and absolute quantification for C3-, SARS-CoV-2–, or C3-/SARS-CoV-2–containing cells were done using the Harmony software (Perkin Elmer, Rodgau, Germany). For quantification analyses, at least 1000 cells per condition were analyzed as indicated.

Real-time RT-PCR for absolute quantification of SARS-CoV-2

SARS-CoV-2 RNA (140 μL) was extracted using FavorPrep Viral RNA Mini Kit (FAVORGEN, Ping-Tung, Taiwan), according to manufacturer's instructions. SARS-CoV-2 levels were quantified using the primer-probe combinations designed by the Centers for Disease Control and Prevention (CDC) 2019-nCoV Real-Time RT-PCR Diagnostic Panel. Sequences specific to 2 distinct regions of the Nucleocapsid (N) gene, N1 and N2, and for the detection of a human housekeeping gene, Ribonuclease P published on the CDC website (https://www.cdc.gov/coronavirus/2019-ncov/lab/rt-pcr-panel-primer-probes.html), were used. Single target assays of all 3 targets were performed in combination with the Luna Universal Probe One-Step RT-qPCR Kit (New England BioLabs, Ipswich, Mass). For absolute quantification using the standard curve method, SARS-CoV-2 RNA was obtained as a PCR standard control from the National Institute for Biological Standards and Control UK (Ridge, UK). The SARS-CoV-2 RNA was used in 10-fold dilutions according to the manufacturer's instructions. All runs were performed on a Bio-Rad CFX 96 instrument and analyzed by the Bio-Rad CFX Maestro 1.1 software (Bio-Rad Laboratories, Hercules, Calif).

Real-time RT-PCR for relative quantification of complement factors

mRNA expressions of C3, C5, C3aR, C5aRI, and C5aRII were analyzed by real-time RT-PCR using commercially available gene-specific primer pairs (PrimePCR, Bio-Rad, Düsseldorf, Germany). mRNA expression of Glycerinaldehyd-3-phosphat-dehydrogenase (PrimePCR, Bio-Rad) served as internal control to quantify the relative gene expression of target genes. The Luna Universal One-Step RT-qPCR kit (New England Biolabs) was used for target amplification, and runs were performed on the CFX96 real-time detection system (Bio-Rad). The cycling conditions were as follows: 10 minutes at 55°C (room temperature), 1 minute at 95°C, 40 cycles: 10 seconds at 95°C, 30 seconds at 60°C. The results were analyzed using the gene expression software of the cycler (CFX Manager Software, ΔΔCt method; BioRad).

Multiparameter flow cytometry

Expression of complement receptors C3aR, C5aRI, and C5aRII was additionally investigated by flow cytometry using a BD FACSVerse analyzer (BD Biosciences, Franklin Lakes, NJ). For this, human airway epithelia (HAE) cultures were treated with commercially available C3aR (SB 290157) and C5aR (mix of W-54011 and DF2593, 1:1) antagonists, both obtained from Sigma-Aldrich. Tissue cultures were treated for 2 hours with 1 μM C3aR or C5aR antagonists before infection with SARS-CoV-2 at a multiplicity of infection (MOI) of 0.1. After infection, cells were washed and cultured for 48 hours. For flow cytometric analyses, cells were harvested using the animal component-free cell dissociation kit (Stemcell, Vancouver, Canada) and stained with a fixable viability dye (BD Horizon, BD Biosciences) as well as antihuman C3aR, C5aRI, and C5aRII mAbs (Biolegend). After fixation, samples were analyzed using BD FACSuite v1.0.6 and BD FACS Diva v9.0 software (BD Biosciences).

Viruses

Clinical specimens from COVID-19–positive swabs (ethics statement, ECS1166/2018) and SARS-CoV-2 viruses from repositories (BEI Resources, Manassas, Va; Center for AIDS Reagents [National Institute for Biological Standards and Control]; Nr-52281, Nr-52282, NR-52286) were propagated according to the manufacturer's instructions and used subsequently to infect HAE tissue cultures.

Profiling of cytokines and anaphylotoxin C3a

The levels of IL-1α, IL-1ra, IL-6, IL-10, GM-CSF, IP-10, MCP-1, RANTES, TSLP, and TNF-α cytokines were measured with FLEXMAP-3D (Luminex, Austin, Tex). Supernatants of HAE cells treated with C5aR and/or SARS-CoV-2 were analyzed, using Magnetic Luminex Multiplex Assay (LXSAHM) from R&D Systems (Minneapolis, Minn), according to the manufacturer's instructions. Final data calculation and analysis was performed in Excel. C3a secretion of HAE tissue models was detected by the BD OptEIA Human C3a ELISA Kit (BD Biosciences) according to the manufacturer's instructions.

Statistical analysis

Statistical analysis of differences in infection levels, TEER values, or cytokine production was performed using the GraphPad prism software and using 1-way ANOVA with Dunnett posttest or unpaired Student *t* test. All experiments (infection experiments, RT-PCR, FACS, plaque assays, TEER measurements) were independently repeated at least 3 times. For quantification of images, at least 2000 cells were analyzed.

RESULTS

SARS-CoV-2 infection significantly increases intracellular C3 levels in primary human airway epithelial cells

To monitor SARS-CoV-2 infection in primary normal human bronchial epithelial cells, monolayers and fully differentiated pseudostratified epithelia were infected using different clinical isolates derived from patients with SARS-CoV-2.[10,11] The clinical specimens were anonymized before use, and the study has been approved by the Ethics Committee of the Medical University of Innsbruck (approval no. ECS1166/2020). In all cases, clear cytopathic effects (CPEs) were apparent, with the attendant detachment/floating of cells and syncytium formation clearly observable in Vero/TMPRSS2 cells (see Fig E1 in this article's Online Repository at www.jacionline.org) as well as in human airway epithelial cells (Fig 1, *A*). Viral RNA copies of clinical specimens and after expansion in Vero/TMPRSS2-expressing cells were absolutely quantified by real-time RT-PCR, and virus titers were found to be 3.16×10^5 to 2.53×10^{12} median $TCID_{50}$ per milliliter (see Fig E2 in this article's Online Repository at www.jacionline.org). HAE cells were infected at an MOI of 0.1, which is consistent with infection by other coronaviruses, such as HCoV-NL63, SARS-CoV, or Middle East respiratory syndrome-related coronavirus and as used in other settings by Zhu et al[18] to determine morphogenesis and CPEs of SARS-CoV-2 infection in HAE.[18-20] HAE cells in monolayers were susceptible to SARS-CoV-2 infection (red) using clinical specimens as a source of the virus (Fig 1, *A*), and surprisingly SARS-CoV-2 infection in these primary airway epithelial cells was accompanied by extensive induction of intracellular (IC) C3 (Fig 1, *A*, and *C*; green). Absolute quantification using less than 1000 cells per condition (UI vs infected with SARS-CoV-2) revealed significantly higher C3 levels in infected cultures, whereas UI cultures exhibited only background IC C3 levels (Fig 1, *A*). Expression of complement components C3 and C5 was analyzed by real-time RT-PCR in UI and SARS-CoV-2–infected HAE cultures (Fig 1,

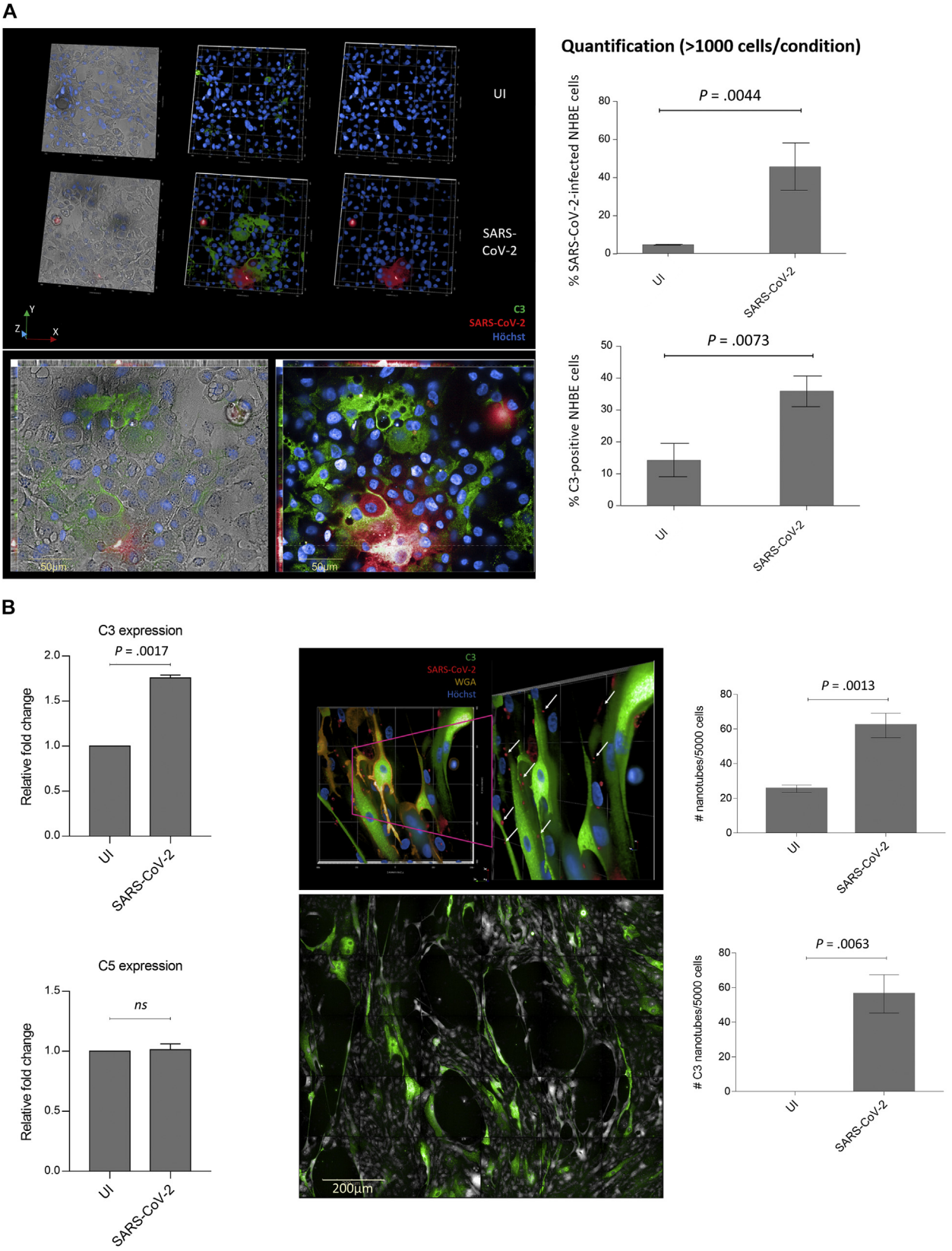

FIG 1. SARS-CoV-2 infection significantly increases intracellular C3 levels in primary HAE cells. **A,** Visualization of complement (green) in SARS-CoV-2 (red)-infected cells imaged by HCS. *Upper panel*, upper images from left to right depict UI cells with BF, Hoechst (blue), and SARS-CoV-2 (red) channels (left), Hoechst, SARS-CoV-2 S1/N, and C3 (green) (middle), and Hoechst and SARS-CoV-2 (right). The *lower panel*

B). Consistent with the microscopic data, expression of C3 was significantly higher in SARS-CoV-2–infected cultures, whereas no differences in expression of C5 were observed (Fig 1, *B*). These analyses demonstrate that intracellular C3 is massively induced at protein and gene expression levels in SARS-CoV-2–infected, primary HAE cultures.

SARS-CoV-2 infection mobilizes intracellular C3 in both infected cells and neighboring cells

Next, we characterized the distribution of intracellular C3 in infected HAE monolayer cultures. We found that IC C3 was produced by infected cells and in particular also their neighboring cells (Fig 1, *C*; green). High- content image analyses revealed that viral particles (Fig 1, *C*, red, arrows) were transmitted in C3-containing, activated cells via membrane nanotube formation to neighboring cells (Fig 1, *C*), a process also used by HIV-1 to exacerbate infection.[21] To quantify nanotubes and C3/SARS-CoV-2–containing nanotubes in UI and SARS-CoV-2–infected cells, digital phase contrast microscopy on a total number of 5000 cells and concomitant analyses using the Harmony software (Perkin Elmer) were performed (Fig 1, *C*, bar graphs). This revealed a significantly higher number of nanotubes and C3/SARS-CoV-2 nanotubes in SARS-CoV-2–infected versus UI cells (Fig 1, *C*, bar graphs). This indicates that SARS-CoV-2 is shuttled via C3-containing nanotubes to neighboring cells.

SARS-CoV-2 generates C3-enriched foci in pseudostratified epithelia

To monitor whether this extensive IC C3 mobilization also occurs within multilayered HAE, 6-month-old, fully differentiated, ciliated, and mucus-producing epithelial tissue models or multiciliated apical-out lung organoids were infected at an MOI of 0.1 with different clinical specimens and infection was monitored using absolute quantitation of SARS-CoV-2-N1 RNA copies, plaque-forming units (PFUs), and high content screening. At day 2 postinfection (2 dpi), whole-tissue cultures or lung organoids were analyzed by real-time RT-PCR (Fig 2, *A*), plaque assays (Fig 2, *B*), and immunofluorescence using various markers (SARS-CoV-2 N/S1; Fig 2, *C*; see Fig E3 in this article's Online Repository at www.jacionline.org; red), C3 (Fig 2, *C*; green), acetylated tubulin (Fig E3; green), MUC5AC (Fig E3; orange), wheat germ agglutinin (Fig 2, *C*; orange), and Hoechst (Fig 2, *C*, and Fig E3; blue). 3D models were highly permissive to SARS-CoV-2 infection as revealed by measuring RNA copy number (Fig 2, *A*, UI 0 copies/mL vs SARS-CoV-2 $\sim 1 \times 10^8$ copies/mL). Also, significantly higher PFU values were detected in Vero/TMPRSS2 cells infected with basolateral supernatants taken 2 dpi from UI or SARS-CoV-2–infected tissue models (Fig 2, *B*, UI 0 PFU/mL vs SARS-CoV-2 ~15,000 PFU/mL).

Immunofluorescence staining revealed a significant infection of the tissue models with SARS-CoV-2 (Fig 2, *C*, and Fig E3, red), with both ciliated and mucus-producing cells being affected by the virus (Fig E3; red). From infected foci, the C3 signal spread over the epithelia to neighboring cells (Fig 2, *C*; green) as was also observed in HAE monolayers. Quantitation of cell numbers in the respiratory tissue models revealed a significant loss of cells in SARS-CoV-2 versus UI on 2 dpi (Fig 2, *D*, first chart, table): 42.3% versus 2.6% of the analyzed cells were positive for C3 in SARS-CoV-2–infected versus UI cultures (Fig 2, *D*, second chart, table); 27% were positive for SARS-CoV-2 in infected cultures; and 3.3% showed background fluorescence staining in UI (Fig 2, *D*, third chart). About half of the SARS-CoV-2–positive cells (15%) were also stained positive for C3 in infected cultures (Fig 2, *D*, fourth chart, table). A total number of more than 5000 cells was analyzed for each condition. 3D and xyz analyses of the 2 signals revealed not only a superficial localization of SARS-CoV-2 and C3 but also that the infection and intracellular complement mobilization penetrated deep into the tissue layers as illustrated in Figure 2, *C* (upper right image). In contrast, only background signals for SARS-CoV-2 and C3 were apparent in the UI control (Fig 2, *C* and D) and these epithelia displayed a higher degree of structural integrity (Fig 2, *C*, lower right image, UI).

Disruption of epithelial integrity is contingent on extensive C3 mobilization, TCC formation, virus release, and C3a secretion

Infection of respiratory tissue models with clinical specimens of SARS-CoV-2 and the concomitant considerable IC C3 mobilization resulted in substantial disruption of the epithelial integrity as assessed by measuring TEER (Fig 3, *A*; left), release of SARS-CoV-2 into the medium (Fig 3, *A*, middle), C3a desArg secretion (Fig 3, *A*, right), and imaging of culture models (Fig 3, *B*). In UI tissue culture, TEER values ranged from 1101 to 1358 Ω/cm^2, whereas this range dropped to 270 to 710 Ω/cm^2 in SARS-CoV-2–infected cells (Fig 3, *A*; left). SARS-CoV-2–infected 3D cultures released significantly higher virus particles into the medium (Fig 3, *A*, left and middle) probably due to extensive syncytium formation[22] and damage of cells as also described in postmortem samples from individuals who died from COVID-19.[23] Moreover, infected cultures secreted significantly higher levels of the anaphylatoxin C3a compared with mock-treated uninfected cultures (Fig 3, *A*, right, UI). Image analyses of SARS-CoV-2–infected cells revealed the disruption of ciliated structures, which were clearly visible in UI models (Fig 3, *B*, wheat germ agglutinin, orange). UI cultures were stained positive for cilia (Fig 3, *B*; upper panel, orange) and nuclei (Fig 3, *B*; upper panel, blue). Furthermore, SARS-CoV-2 was not detected in UI

represents a zoomed-in view of a region of SARS-CoV-2–infected HAE cells with BF shown in addition to the 3 fluorescence channels on the left and the fluorescence channels alone on the right. Quantification of infection and C3 levels in UI and SARS-CoV-2–infected cells (>1000 cells) are depicted on the right. **B,** Expression of complement components C3 and C5 was analyzed by real-time RT-PCR in UI and SARS-CoV-2–infected HAE cultures. Three independent experiments were performed in duplicate. **C,** Nanotube formation and quantification of C3 (green)-containing nanotubes (DPC) in UI and SARS-CoV-2–infected cells were performed using HCS and counting 5000 cells per condition. Experiments were performed for a minimum of 3 independent replicates, and statistical significance was analyzed using GraphPad Prism software and unpaired Student *t* test. *BF,* Brightfield; *DPC,* digital phase contrast; *HCS,* high content screening.

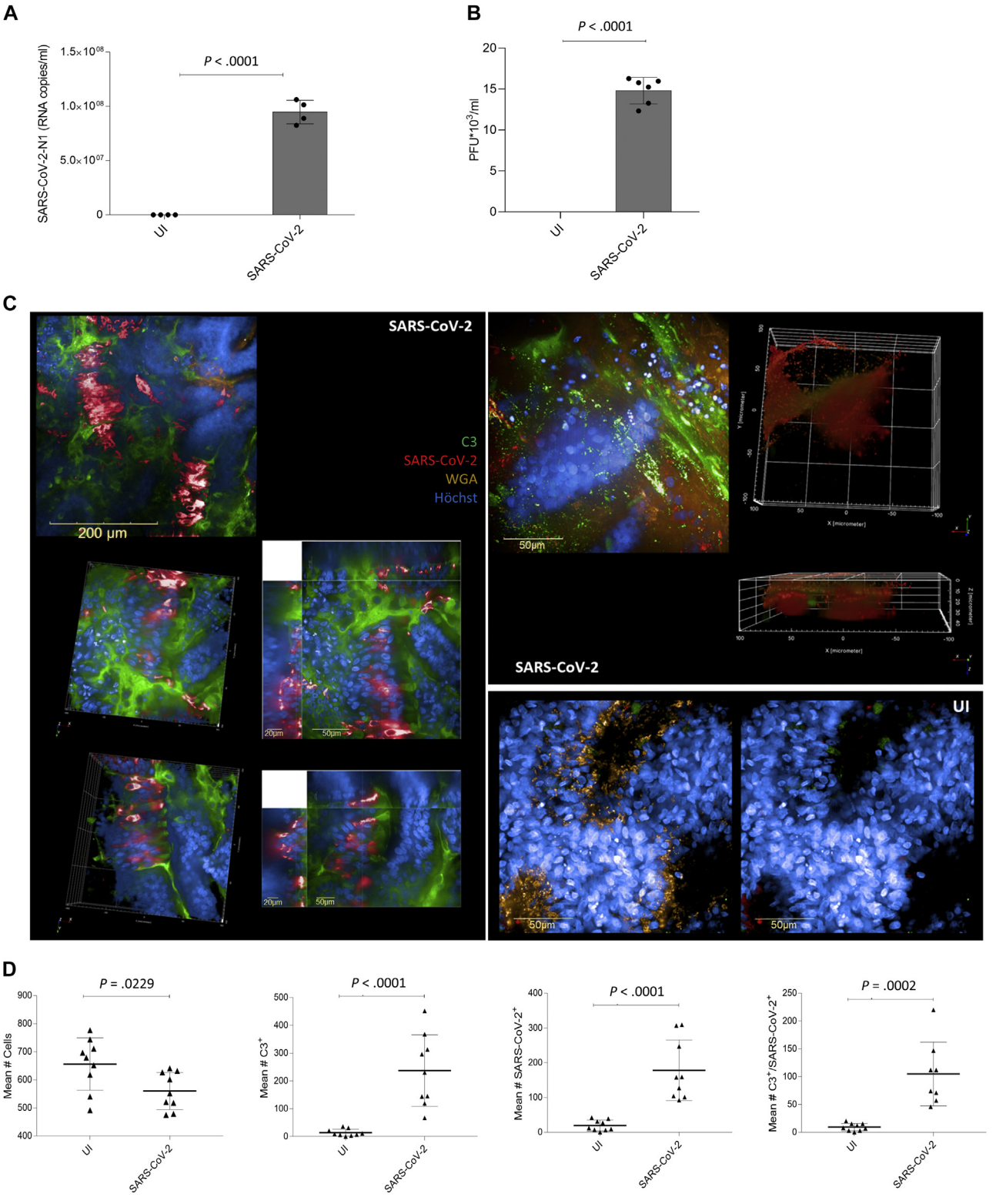

	∑ Cells (%)	∑ C3⁺ cells (%)	∑ SARS-CoV-2⁺ cells (%)	∑ C3/SARS-CoV-2⁺ cells (%)
UI	5910 (100%)	124 (2.6%)	173 (3.3%)	83 (1.73%)
SARS-CoV-2	5047 (100%)	2134 (42.3%)	1357 (27%)	756 (15%)

FIG 2. SARS-CoV-2 effectively infects pseudostratified epithelia and generates C3-enriched foci. **A,** 3D lung models are highly permissive for SARS-CoV-2 infection and depict 1×10^8 RNA copies/mL of SARS-CoV-2-

cells when using Alexa594-labeled antibodies recognizing the spike 1 (S1) or nucleocapsid (N) proteins (Fig 3, *B*; upper panel, red). Only background levels of C3 were detectable in UI cultures (Fig 3, *B*, upper panel, green). In contrast, ciliated structures were destroyed in SARS-CoV-2–infected cultures and became apparent already at 2 dpi (Fig 3, *B*; middle panel, orange) and were aggravated by ongoing infection and illustrated at 5 dpi (Fig 3, *B*; lower panel, orange). Infected cultures stained positive for the S1 and N proteins of SARS-CoV-2 (Fig 3, *B*; red), and C3 (Fig 3, *B*; green) was heavily induced in such tissue models. To further characterize whether MAC membrane channels might be involved in decreased epithelial resistance, we stained UI and SARS-CoV-2–infected cultures using an anti–C5b-9 antibody recognizing a neoepitope exposed on polymerized C9 when incorporated in the human TCC.[17] The C5b-9 antibody colocalized in many SARS-CoV-2–infected cells (Fig 3, *C*, white arrows, and Fig 3, *D*, SARS-CoV-2), whereas in UI cultures only background signals were obtained using these antibodies (Fig 3, *C* and *D*, UI). Brightfield images (Fig 3, *C*, left), staining of acetylated tubulin-recognizing ciliary structures (Fig 3, *C*, right, pink), and C5b-9–single positive cells (Fig 3, *C*, right, green arrows) additionally illustrated rounding up of cells and loss of structured cilia in infected cultures. All experiments were independently repeated at least 3 times, and quantitation was performed in 4 different fields on at least 2000 cells (Fig 3, *D*). These data revealed that local complement activation in pseudostratified HAE cells correlated with the disruption of the epithelial integrity following SARS-CoV-2 infection.

Effective reduction of local complement after SARS-CoV-2 infection by antagonizing of C3aR or C5aR on HAE cells

Next, we used our highly differentiated HAE model to investigate possible treatment options that might circumvent the induction of the synthesis of complement proteins by SARS-CoV-2, productive virus infection, and the concomitant secretion of high levels of anaphylatoxin and associated tissue disruption. To this end, we performed microscopic analyses and real-time RT-PCR of culture models as well as plaque assays of basolateral supernatants from the same cultures pretreated with C3aR or C5aR inhibitors on the basolateral side before addition of SARS-CoV-2 clinical isolates at an MOI 0.1 on the apical side. Before antagonizing C3aR and C5aR on HAE cells, we characterized C3aR, C5aR1, and C5aR2 expression on HAE monolayers by flow cytometry (see Fig E4 in this article's Online Repository at www.jacionline.org) and 3D tissue models by high content screening (see Fig E5 in this article's Online Repository at www.jacionline.org). High C5aR2 expression was determined on both monolayers and tissues (Figs E4 and E5), whereas C3aR and C5aR1 were expressed only on 3D models (Fig E5). After verifying the presence of the various anaphylatoxin receptors in our system, cells were infected for 2 days and then stained for SARS-CoV-2 S1/N (red), intracellular C3 (green), and nuclei (blue) for microscopic analyses (Fig 4, *A*). As demostrated before, SARS-CoV-2–infected HAE tissue models showed a high level of infection (Fig 4, *A*; SARS-CoV-2, red) and intracellular C3 induction (Fig 4, *A*; SARS-CoV-2, green) as well as disruption of the epithelium compared with the uninfected cultures (Fig 4, *A*; UI). Basolateral preincubation of epithelia with C3aR antagonist resulted in reduction of viral loads as well as of C3-positive cells and preserved a more intact morphology of the human airway epithelium (Fig 4, *A*; C3aR-Inh/SARS-CoV-2). In addition to imaging analyses, basolateral supernatants of pretreated and infected HAE cultures were harvested on 2 dpi to perform a plaque assay using TMPRSS2-expressing VeroE6 (VeroE6/TMPRSS2) cells for determining viral infectivity from these cultures (Fig 4, *B*). Furthermore, the virus concentration was analyzed by quantitative real-time RT-PCR (Fig 4, *C*). Both plaque assay and real-time RT-PCR revealed a slight decrease in PFUs or SARS-CoV-2 copy numbers after treatment with C3aR antagonist (C3aR Inh/SARS-CoV-2), but compared with nontreated, infected cells (SARS-CoV-2) this reduction was statistically not significant (Fig 4, *B* and C).The most convincing results in terms of antagonizing SARS-CoV-2–mediated intracellular C3 production were achieved using a C5aR antagonist (Fig 4, *A-D*; C5aR Inh/SARS-CoV-2). Only background levels of virus-infected cells comparable to the background signal in UI cultures were detected (red) and tissue integrity was maintained in C5aR antagonist–treated, SARS-CoV-2–infected HAE cultures (Fig 4, *A*; C5aR Inh/SARS-CoV-2). Similar results were also obtained from plaque assays and RT-PCR (Fig 4, *B* and *C*). Pretreatment of HAE cultures with C5aR antagonist (C5aR Inh/SARS-CoV-2) significantly reduced viral titers compared with infected cultures (SARS-CoV-2) in basolateral supernatants (Fig 4, *B*) and also led to a reduced number of infective viral particles (Fig 4, *C*). Compared with SARS-CoV-2–infected cultures, we found a highly significant reduction in C3a desArg in both C3aR- and C5aR antagonist–treated and SARS-CoV–2 infected cells (Fig 4, *D*; C3aR Inh/SARS-CoV-2 and C5aR Inh/SARS-CoV-2). Blocking C5aR on HAE cells that were subsequently infected with SARS-CoV-2 resulted in a significant decrease in C3a desArg levels compared with HAE cultures pretreated with C3aR inhibitor and then infected, confirming the results seen in imaging analyses (Fig 4, *D*; C3aR Inh/SARS-CoV-2 and C5aR Inh/SARS-CoV-2). Here, we illustrated that SARS-CoV-2–induced excessive local complement activation can be decreased by antagonizing C3aR and is completely reversed by blocking C5aR.

N1 on 2 dpi. No viral RNA was analyzed in UI tissues. Four independent experiments were performed, and statistical significance was analyzed using unpaired Student *t* test. **B,** Plaque assays of SARS-CoV-2 supernatants from HAE cells were performed on Vero/TMPRSS2 cells. Assays were independently repeated 6 times, and unpaired Student *t* test was performed to evaluate statistical significance. **C,** Multilayered epithelia were infected using SARS-CoV-2. On 2 dpi, tissues were stained for Hoechst (blue), SARS-CoV-2 S1/N (red), complement C3 (green), and WGA (orange). Representative images of infected regions and 3D and xyz high content imaging are shown on the left and upper right. Lower right, uninfected 3D pseudostratified epithelia were stained as controls. Experiments were performed at least 4 times and representative images are shown. **D,** Absolute quantification of total cell numbers (first panel), C3- (second panel), SARS-CoV-2–positive cells (third panel), and C3/SARS-CoV-2, double-positive cells (fourth panel) was performed in UI and SARS-CoV-2–infected cultures. Per condition, about 6000 cells were analyzed and statistical significance evaluated using an unpaired Student *t* test. *WGA*, Wheat germ agglutinin.

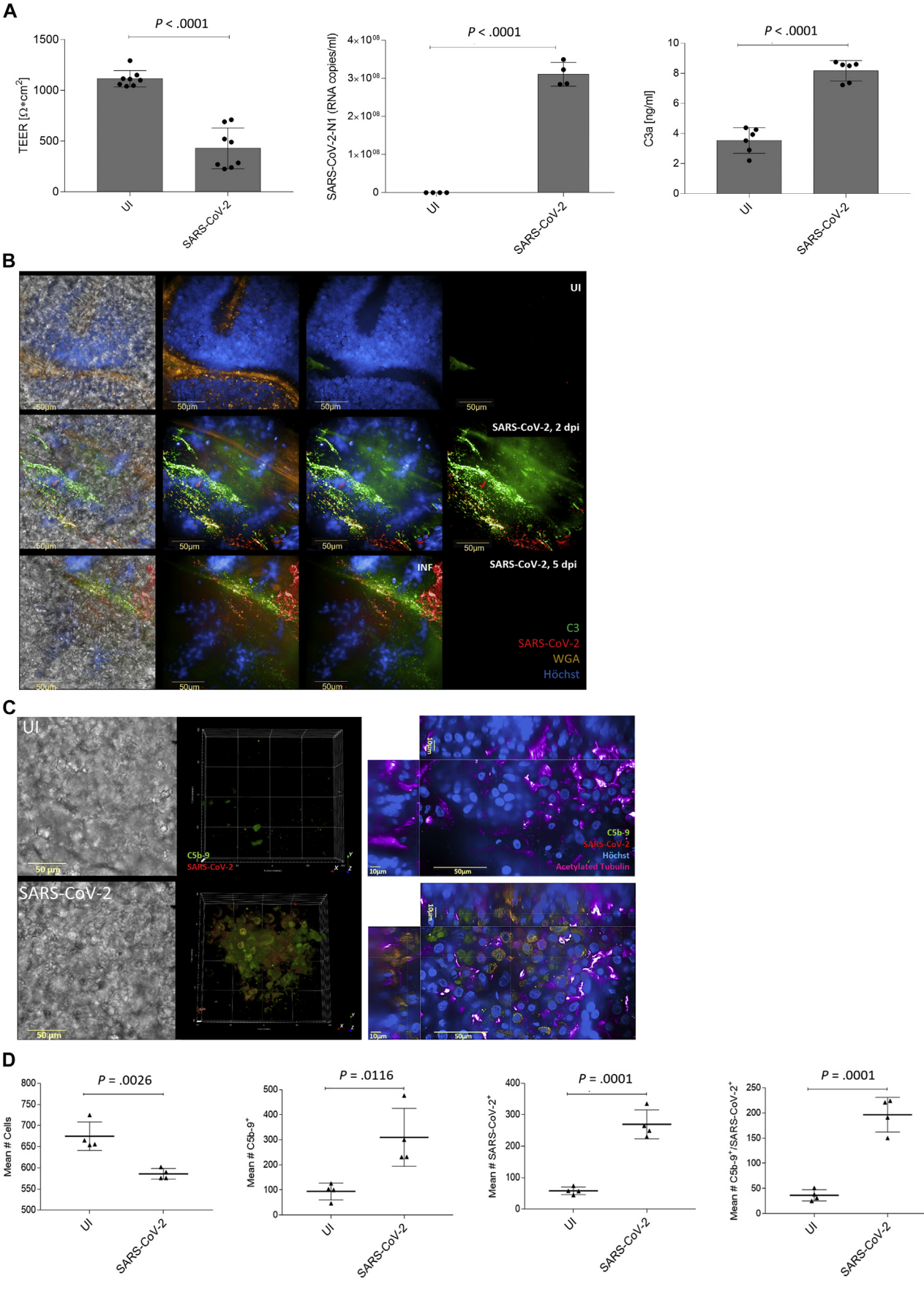
A
P < .0001
TEER [Ω*cm²]
1500
1000
500
0
UI
SARS-CoV-2
P < .0001
SARS-CoV-2-N1 (RNA copies/ml)
4×10⁰⁸
3×10⁰⁸
2×10⁰⁸
1×10⁰⁸
0
UI
SARS-CoV-2
P < .0001
C3a [ng/ml]
10
8
6
4
2
0
UI
SARS-CoV-2
B
UI
SARS-CoV-2, 2 dpi
SARS-CoV-2, 5 dpi
INF
C3
SARS-CoV-2
WGA
Höchst
50µm
C
UI
SARS-CoV-2
C5b-9
SARS-CoV-2
Höchst
Acetylated Tubulin
50 µm
10µm
50µm
D
P = .0026
Mean # Cells
800
750
700
650
600
550
500
UI
SARS-CoV-2
P = .0116
Mean # C5b-9⁺
500
400
300
200
100
0
UI
SARS-CoV-2
P = .0001
Mean # SARS-CoV-2⁺
400
300
200
100
0
UI
SARS-CoV-2
P = .0001
Mean # C5b-9⁺/SARS-CoV-2⁺
250
200
150
100
50
0
UI
SARS-CoV-2

Protection against SARS-CoV-2 infection by inhibiting C5aR

To determine whether C3aR/C5aR antagonism is potentially an effective postexposure preventative mechanism, we infected differentiated HAE tissue models with SARS-CoV-2 clinical isolates and added the C3aR and C5aR antagonists following a 6-hour delay. Cells were again analyzed after 2 days. As depicted in Fig 5, *A*, SARS-CoV-2 efficiently infected the culture models and caused tissue disruption (Fig 5, *A*; SARS-CoV-2), whereas uninfected control cells displayed an intact tissue morphology as illustrated by a uniform phalloidin staining without disruptions (Fig 5, *A*; UI). Addition of C3aR inhibitor (Fig 5, *A*; C3aR Inh/SARS-CoV-2) led to decreased viral load, but the reduction in local C3 production was not as obvious as that observed on preadministration of antagonist. C5aR antagonism resulted in decreased SARS-CoV-2 infection and lower C3 levels (Fig 5, *A*; C5aR Inh/SARS-CoV-2). To investigate whether the delayed C3aR/C5aR antagonism is also associated with protection from SARS-CoV-2 infection, TMPRSS2-expressing VeroE6 (VeroE6/TMPRSS2) cells were infected using the supernatants from such differentially treated HAE cells. Cells were monitored for CPEs. Clear CPEs with detachment/floating and syncytium formation developed 1 dpi, and all cells were detached in SARS-CoV-2 and surprisingly also in C3aR antagonist–/SARS-CoV-2–exposed cells on 2 dpi. In contrast, antagonizing C5aR protected the cells from CPEs after SARS-CoV-2 infection and they looked similar to uninfected controls (Fig 5, *B*) and C5aR antagonist–treated control cells (not shown). Hence, we showed that inhibiting C5aR on fully differentiated HAE cells prevented subsequent productive SARS-CoV-2 infection in highly susceptible cells.

Maintaining epithelial integrity following SARS-CoV-2 infection by inhibition of C5aR on differentiated HAE cells

Because C5aR antagonism appeared to be the most promising strategy for protection against SARS-CoV-2 infection due to the downregulation of local complement activation, we performed more detailed analyses in such cultures to account for the absence of infection observed in susceptible indicator cells. We found that TEER values could be restored in SARS-CoV-2–infected HAE cells treated with C5aR inhibitor (Fig 6, *A*). Although tissue models were strongly disrupted on SARS-CoV-2 infection as indicated by a significantly lower TEER value compared with UI (Fig 6, *A*; UI), a highly significant improvement in epithelial integrity was observed in C5aR-treated as well as C5aR- and SARS-CoV-2–exposed cultures (Fig 6, *A*; C5aR Inh and C5aR Inh/SARS-CoV-2). Also, C3-containing nanotube levels were reduced to zero in HAE cultures pretreated with C5aR antagonist before SARS-CoV-2 infection comparable to UI and C5aR Inh/UI and in contrast to SARS-CoV-2–infected cultures (Fig 6, *B*). To further characterize whether C5a alone can mediate damage of HAE cultures, cells were treated with 1 μg/mL C5a for 24 hours, but not infected with SARS-CoV-2 (Fig 6, *C*). These experiments revealed that TEER values of HAE tissues significantly dropped on treatment with C5a compared with untreated control cells (Fig 6, *B*, UI), and microscopic analyses also showed disruption of tissue integrity of these cultures (see Fig E6 in this article's Online Repository at www.jacionline.org). This pointed toward a role of local complement activation in amplifying viral load and worsening tissue injury in patients with COVID-19.

C5aR antagonism correlates with downmodulation of the proinflammatory signature following SARS-CoV-2 infection

Finally, we analyzed the proinflammatory signature of HAE tissue cultures during SARS-CoV-2 infection in the presence and absence of C5aR antagonist. As controls, tissue models were left untreated (UI) or treated with C5aR inhibitor only (C5aR Inh/UI) (Fig 6, *D*). As assessed by luminex technology and median fluorescence intensities, SARS-CoV-2 induced significantly higher levels of IL-6, MCP-1, IL-1α, and RANTES compared with uninfected control cultures (Fig 6, *D*; SARS-CoV-2 vs UI). IP10 levels fluctuated in various experiments following SARS-CoV-2 infection, with an overall modest decrease observed in C5aR Inh–pretreated cultures (Fig 6, *D*). Induction of all proinflammatory cytokines by SARS-CoV-2 infection was reversed by antagonizing C5aR, and such pretreated cultures showed levels similar to uninfected cultures (Fig 6, *D*; C5aR Inh/SARS-Cov-2 and UI, C5aR Inh/UI). Blocking C5aR may therefore be a possible treatment option that could prevent exaggerated anaphylatoxin and cytokine responses and eventually bring the viral load under control due to the maintenance of an intact epithelium.

DISCUSSION

The entire airway epithelium from the nasal cavity down to the alveoli constantly encounters pathogens and if invaders are able to breach the mucus-producing, ciliated, pseudostratified barrier, an immediate innate immune response is needed. In this context, complement proteins have been demonstrated to be produced and secreted by airway epithelial cells.[24] Clinical evidence has been provided that complement may play a pathogenic role in COVID-19, and recently Yan et al[8] illustrated that SARS-CoV-2 infection augments C3 gene transcription locally in lung epithelial cells and that SARS-CoV-2–induced C3 results in local biologically active C3 products.[8] Normally, complement should be

FIG 3. Disruption of epithelial integrity is a combination of extensive C3 mobilization, C3a secretion, TCC formation, and virus production. **A,** TEER in Ω/cm^2 (left), SARS-CoV-2-RNA copy numbers/mL (middle), and C3a (right) levels were determined for both UI and SARS-CoV-2–infected 3D airway epithelia and plotted on a bar graph. Four to 8 independent experiments were performed, and statistical significance was analyzed using unpaired Student *t* test. **B,** 3D airway epithelia were fixed and stained for Hoechst (blue), SARS-CoV-2-S1/N (red), C3 (green), and WGA (orange) and analyzed at 2 (middle panel) and 5 dpi (lower panel). The upper row represents UI cells. Experiments were independently repeated 3 times, various fields were analyzed, and representative images are shown. **C,** Multilayered epithelia were stained using C5b-9 Ab (green), SARS-CoV-2 (red), Hoechst (blue), and acetylated tubulin (pink) in UI and SARS-CoV-2–infected cultures. The experiment was repeated 3 times, and representative BF, 3D, and xyz stacks are illustrated. **D,** Absolute quantification of total cell numbers (first panel), C5b-9– (second panel), SARS-CoV-2–positive cells (third panel), and C5b-9/SARS-CoV-2 double-positive cells (fourth panel) was performed in UI and SARS-CoV-2–infected cultures. Per condition, more than 2000 cells were analyzed and statistical significance evaluated using an unpaired Student *t* test. *BF*, Brightfield; *WGA*, wheat germ agglutinin.

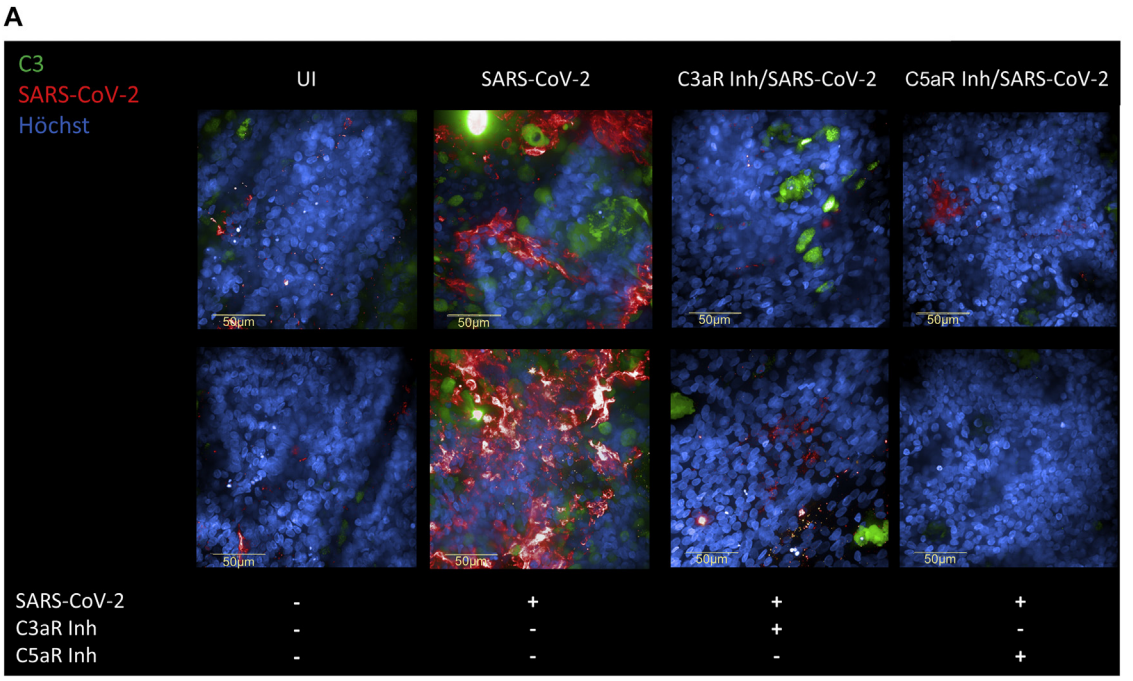
A
C3
SARS-CoV-2
Höchst
UI
SARS-CoV-2
C3aR Inh/SARS-CoV-2
C5aR Inh/SARS-CoV-2
50µm
SARS-CoV-2 - + + +
C3aR Inh - - + -
C5aR Inh - - - +

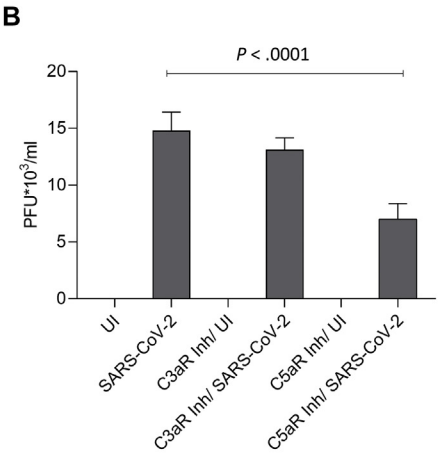
B
P < .0001
PFU*10³/ml
20
15
10
5
0
UI
SARS-CoV-2
C3aR Inh/ UI
C3aR Inh/ SARS-CoV-2
C5aR Inh/ UI
C5aR Inh/ SARS-CoV-2

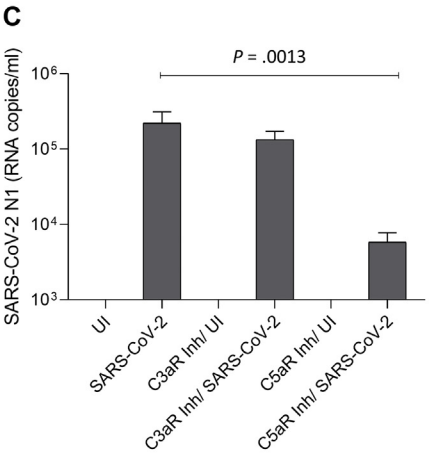
C
P = .0013
SARS-CoV-2 N1 (RNA copies/ml)
10⁶
10⁵
10⁴
10³
UI
SARS-CoV-2
C3aR Inh/ UI
C3aR Inh/ SARS-CoV-2
C5aR Inh/ UI
C5aR Inh/ SARS-CoV-2

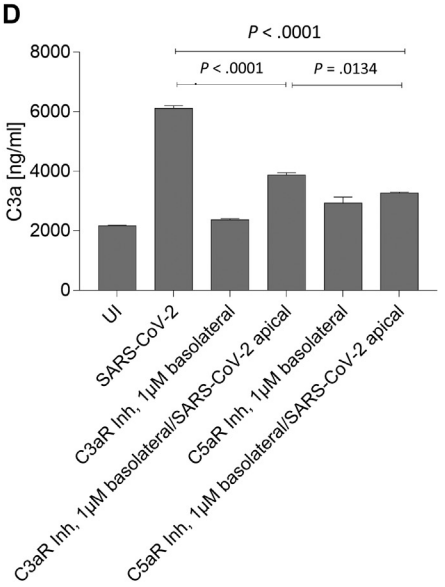
D
P < .0001
P < .0001
P = .0134
C3a [ng/ml]
8000
6000
4000
2000
0
UI
SARS-CoV-2
C3aR Inh, 1µM basolateral
C3aR Inh, 1µM basolateral/SARS-CoV-2 apical
C5aR Inh, 1µM basolateral
C5aR Inh, 1µM basolateral/SARS-CoV-2 apical

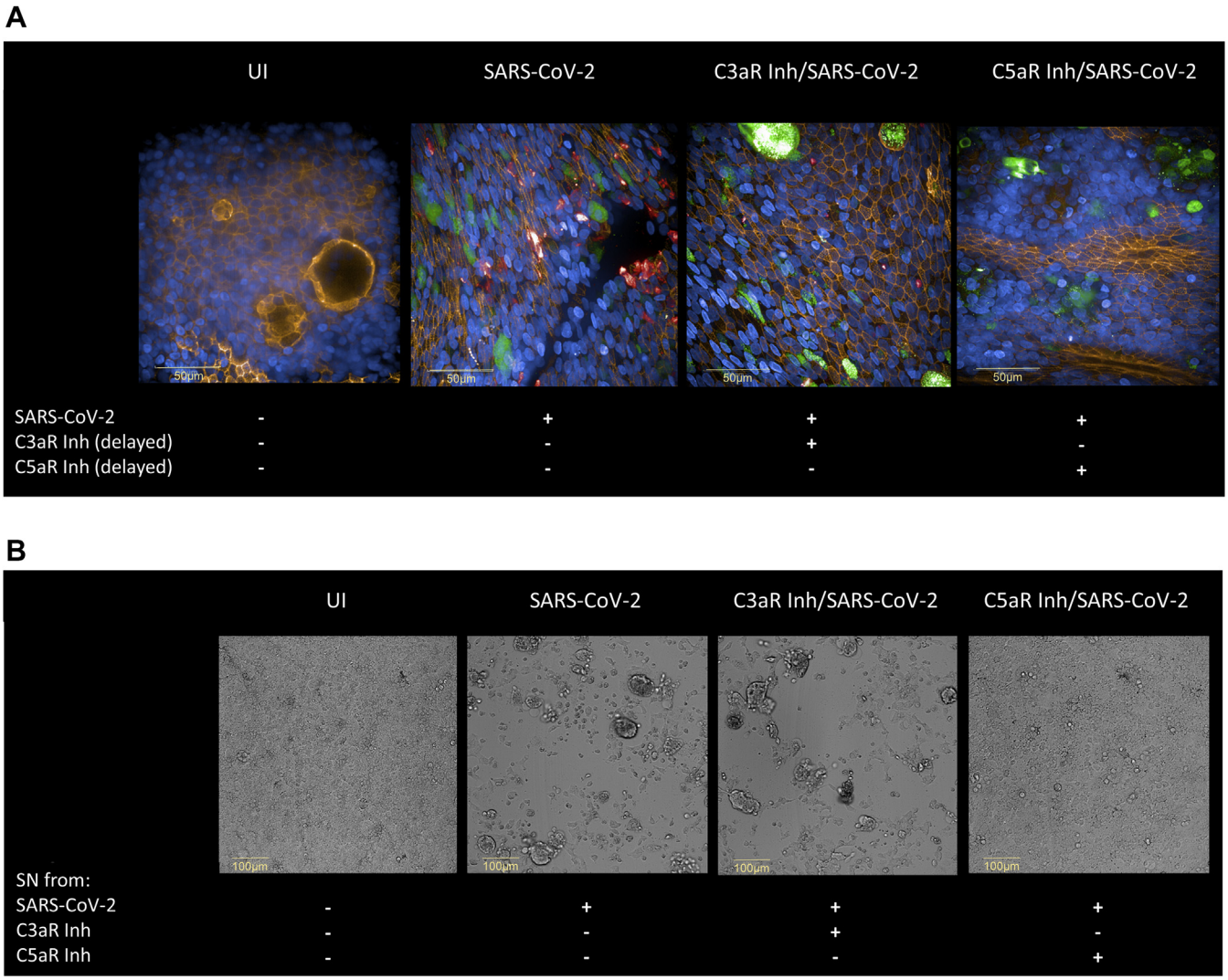

FIG 5. Protection against SARS-CoV-2 infection by inhibiting C5aR. **A,** Visualization of SARS-CoV-2–infected pseudostratified epithelia treated 6 hours postinfection with 1 μM C3a (SB 290157) or 1 μM C5aR (mix of W-54011 and DF2593, 1:1) inhibitors. Multilayered epithelia were infected by apical addition of SARS-CoV-2 (MOI 0.1-1) and after 6 hours C3aR Inh or C5aR Inh was administered basolaterally. Cells (2 dpi) were fixed and stained for Hoechst (blue), SARS-CoV-2 S1/N (red), complement C3 (green), and phalloidin (orange) and then analyzed by confocal microscopy. Different experimental conditions are indicated by the white text underneath the images. **B,** BF microscopy analysis of VeroE6/TMPRSS2 cells reinfected with supernatants SARS-CoV-2–infected pseudostratified epithelia treated 6 hours postinfection with C3aR or C5a receptor inhibitors. Supernatants from SARS-CoV-2–infected pseudostratified epithelia treated 6 hours postinfection with C3aR or C5a receptor inhibitors were used to infect VeroE6/TMPRSS2 cells, which were fixed and visualized by BF confocal microscopy 2 dpi. Text underneath images indicates the corresponding experimental conditions. Independent experiments were repeated at least 3 times. *BF*, Brightfield.

FIG 4. Effective reduction of local complement after SARS-CoV-2 infection by antagonizing of C3aR or C5aR on HAE cells. **A,** Multilayered epithelia were pretreated for 2 hours with 1 μM C3aR (SB 290157) or 1 μM C5aR (mix of W-54011 and DF2593, 1:1) inhibitors added basolaterally and infected apically using SARS-CoV-2 (MOI 0.1-1). Cells were fixed and stained for Hoechst (blue), SARS-CoV-2 S1/N (red), and C3 (green) on 2 dpi. Two independent experiments are shown (upper and lower panels) **B,** Plaque assays of supernatants from UI and infected cultures plus/minus C3aR and C5aR inhibitor were performed on Vero/TMPRSS2 cells. Assays were independently repeated 3 times, and 1-way ANOVA using Dunnett posttest was performed to evaluate statistical significance. **C,** Viral RNA was analyzed in UI and infected tissues plus/minus inhibitors. The experiment was repeated thrice, and 1-way ANOVA using Dunnett posttest was performed. **D,** C3a level determination in C3aR Inh– and C5aR Inh–treated SARS-CoV-2–infected pseudostratified epithelia. Basolateral supernatants (2 dpi) were harvested and C3a levels determined using a BD Biosciences OptEIA Human C3a ELISA kit. C3a levels (ng/mL) were determined for each experimental condition and plotted on a bar graph.

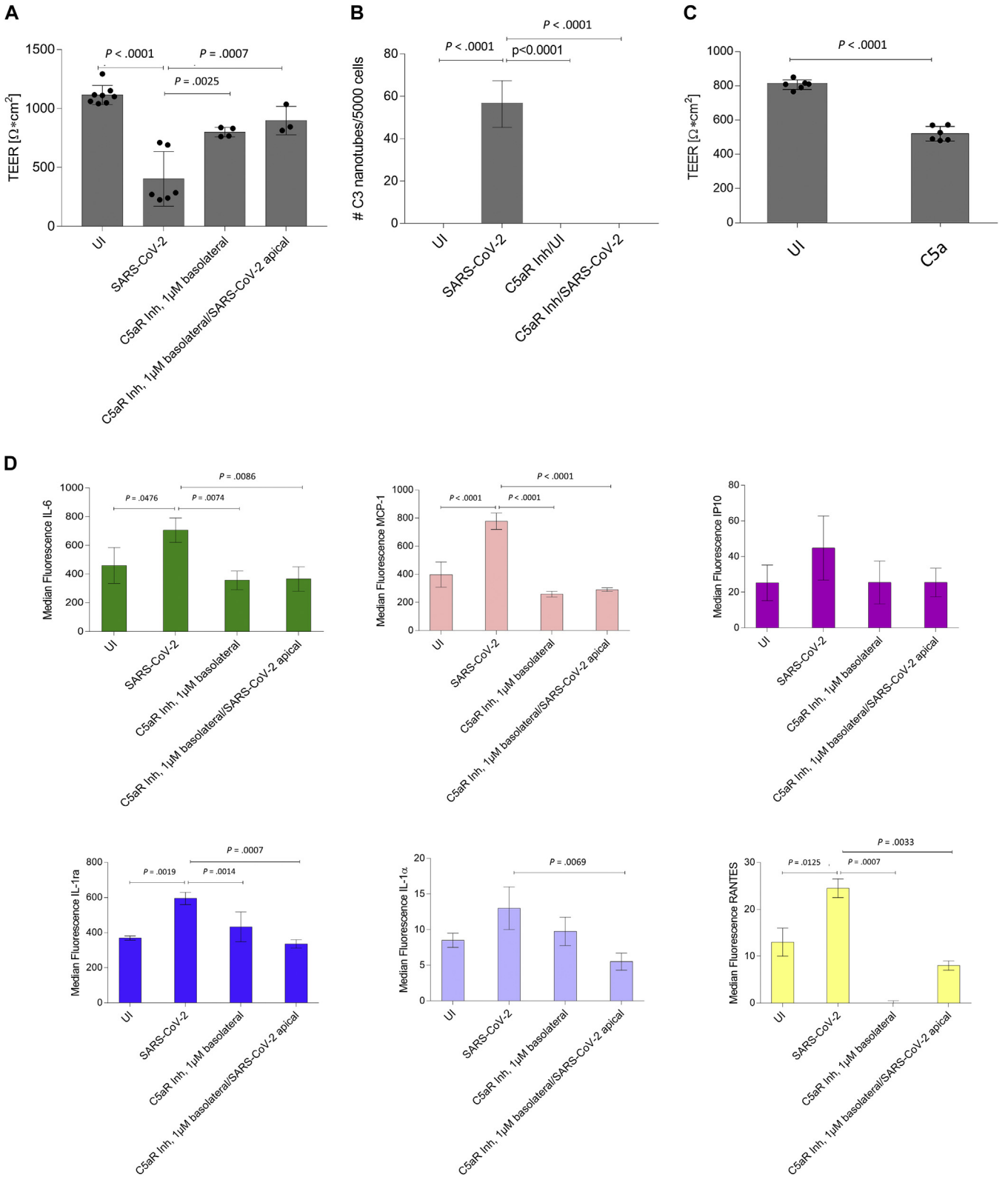

FIG 6. Maintenance of epithelial integrity and reduced proinflammatory response of SARS-CoV-2–infected cells treated with C5aR inhibitor. **A,** Multilayered epithelia were infected by apical addition of SARS-CoV-2 (MOI 0.1-1) and following 6 hours were then supplemented basolaterally with either 1 μM C3aR (SB 290157) inhibitor or 1 μM C5aR (mix of W-54011 and DF2593, 1:1) inhibitor. TEER measurement was performed on 2 dpi for each experimental condition, and the results were plotted on a bar graph. Experiments were performed thrice and statistical significance evaluated using 1-way ANOVA and Dunnett posttest. **B,** C3-containing nanotubes were reduced to zero in C5aR inhibitor–treated cultures also on SARS-CoV-2 infection

protective during viral infections, but with respect to COVID-19 local complement activation might worsen tissue injury.[25,26] Here, we found that exaggerated C3 production, C3a desArg secretion, and TCC formation in SARS-CoV-2–infected primary human airway epithelial tissue cultures initiated a highly inflammatory microenvironment, resulting in significant tissue damage despite the lack of other immune components. Also, neighboring cells not directly infected with SARS-CoV-2 showed elevated amounts of C3 as well as TCC staining, which might indicate dead or damaged cells. On interaction of SARS-CoV-2 with pseudostratified epithelia, a massive intracellular C3 production was observed with concomitant secretion of the anaphylatoxin C3a desArg, formation of TCC and release of virions, destruction of tissue culture integrity, and hyperactivation of proinflammatory cytokines (IL-6, MCP-1, IL-1α, RANTES). This could be reversed by blocking C5aR localized to primary human airway epithelial cells, which completely antagonized virus-induced tissue damage, virus replication as analyzed by viral RNA in supernatants and plaque assays, and local complement activation, even if added after infection of pseudostratisfied epithelia with SARS-CoV-2.

Treatment of 5 severely ill COVID-19 patients with the C3 antagonist AMY-1 or adjunct treatment with the C5 activation inhibitor eculizumab resulted in disease recovery and point toward a pathogenic role of locally produced complement during COVID-19.[27] A study using human immune cells and human C5aR1 knock-in mice demonstrated that anti-C5aR1 therapeutic mAbs prevented C5a-mediated activation and recruitment of cells and inhibited acute lung injury.[25] Worsening of injury by local complement activation in the airway epithelium was already shown for SARS-CoV infection. In addition, increased C3a and C5a levels in plasma and lung homogenates have been implicated in the pathogenesis of various lung conditions including cystic fibrosis and idiopathic pulmonary fibrosis.[28,29] Thus, increased anaphylatoxin levels resulted in downmodulation of regulators of complement activation such as CD55 and CD46 and changes in injury markers on HAE cells, such as decreased E-cadherin, and increased cleaved poly-ADP ribose polymerase.[28] Furthermore, in patients with idiopathic lung injury, increased soluble C5b-9 levels were analyzed in lung lavage fluid.[24] We, too, found a significantly enhanced induction of TCC formation in SARS-CoV-2–infected tissue models compared with UI controls, suggesting that cell damage also occurs by formation of MAC membrane channels in infected cells. In addition, inhibition of C3aR or C5aR in bleomycin-injured mice with fibrotic lungs led to downregulation of local complement production as well as disease progression.[24,30] Here, we demonstrated that local complement production and progression of SARS-CoV-2 infection could be arrested in primary HAE by C5aR antagonist. This was even the case if the C5aR blocker was administered several hours after SARS-CoV-2 infection. Besides decreasing locally produced complement, blocking C5aR resulted in the restoration of transepithelial electrical resistance, a marker of epithelial integrity. Furthermore, we observed a normalization of proinflammatory cytokine levels back to those of healthy untreated HAE tissue models or cultures incubated with the antagonists alone. In COVID-19–positive individuals, the levels of 10 circulating cytokines (IL-1α, IL-1RA, IL-6, IL-10, GM-CSF, IP-10, MCP-1, RANTES, TSLP, and TNF-α) were reported as being significantly elevated, and different expression profiles were associated with different disease severity.[31] Inflammation is among the first coordinated lines of defense following tissue damage by either infection or injury, but excessive immune responses convert the protective mechanism into a harmful one as observed in patients with COVID-19.[32] Besides the aforementioned biomarkers for disease severity, the anaphylatoxins C3a and C5a secreted by airway epithelial cells or C3 in mucus might also serve as valuable indicators for disease severity or progression. As illustrated in our highly differentiated, pseudostratified HAE, extremely high levels of C3a desArg are secreted from the airway epithelium on interaction with SARS-CoV-2. Both C3a desArg and C5a comprise important effector molecules attracting, activating, and regulating components of innate and adaptive immunity.[33] C5a was demonstrated to induce expression of IL-1β and IL-8 in mononuclear cells and augments the release of IL-6 and TNF-α.[34] Furthermore, several studies illustrated that C5a and C5aR may be responsible for inflammation in the lung, that is, during IgG-mediated inflammation or during ARDS,[35,36] and blocking C5aR attenuated IgG-complex–mediated inflammation. Although we were not able to detect C5a in basolateral supernatants of SARS-CoV-2–infected epithelia, this observation might be attributable to its previously described intracellular engagement and capacity to activate C5aR1 and induction of inflammasome activity.[37] Although this "complement-metabolism-inflammasome" axis (reviewed in Arbore et al[38]) was first demonstrated in immune cells such as $CD4^+$ T cells, it is also conceivable that such pathway is also activated in the airway epithelium, showing expression of C5aR1 at the protein and the mRNA levels.[39,40] Herein, all anaphylatoxin receptors (C3aR, C5aR1, C5aR2) were shown to be expressed on 3D ALI tissue models. As recently reviewed in Kulkarni et al,[41] all components of lectin and alternative complement pathways are expressed in or produced by human airway epithelial cells, making it likely that on SARS-CoV-2 infection, exacerbating or chronic amplification of local synthesis of these complement proteins putatively propagates epithelial injury. Furthermore, we found a significantly higher expression of proinflammatory cytokines following stimulation of HAE tissue models with SARS-CoV-2, which is in line with C5a effector functions. Importantly, the upregulation of proinflammatory cytokines IL-6, MCP-1, IL-1α, or RANTES was efficiently blocked by C5aR antagonism. Besides C5a, C3a desArg may bind C5aR2 at a site distinct from the C5a binding site,[42-44] but this issue was controversially discussed over years[45] as well as the role of C5aR2 as either immune-activating or immune-dampening (reviewed in Li et al[46]). Because we found

(C5aR Inh/SARS-CoV-2). A total of 5000 cells were counted for their presence of nanotubes (DPC), C3, and SARS-CoV-2 under the indicated conditions. **C,** Addition of recombinant C5a significantly reduced the epithelial integrity as analyzed by TEER. Experiments were performed thrice and statistical significance evaluated using unpaired Student *t* test. **D,** Supernatants from SARS-CoV-2–infected pseudostratified epithelia subsequently treated with C5aR antagonists were harvested 2 dpi and cytokine profiles determined using Luminex technology. Levels of cytokines are expressed in median fluorescence intensities. Two independent experiments in duplicate were performed. Statistical significance was evaluated using 1-way ANOVA and Dunnett posttest. *DPC,* Digital phase contrast.

a highly elevated induction of C3a desArg on SARS-CoV-2 infection and abundant expression of C5aR2, some of the observed effects may be due to interaction of these complement components. More detailed analyses of these interactions during SARS-CoV-2 infection are necessary, but would have exceeded the scope of this study. Yet, these data provide a promising base for future translational studies of modifying C3a desArg or C5a/C5a desArg and C5aR1 or C5aR2 interactions.

Conclusions

We propose that the application of complement inhibitors represents a promising approach in SARS-CoV-2 disease management. Complement inhibitors (eg, AMY-101, eculizumab, or its variant ravulizumab) are currently in advanced stages of SARS-CoV-2 clinical trials and can be administered to the lungs through nebulizers.[47-49] Beside anaphylatoxin targeting, another yet unexplored option is the targeting of regulators of complement activation such as CD46 or CD55 in the lungs of patients with COVID-19 to reduce inflammation.[48,50] As illustrated herein and also reviewed in Jodele and Koehl,[7] complement may serve as a powerful new therapeutic target for COVID-19 treatment, because severely ill patients with COVID-19 with atypical ARDS showed an extensive complement activation both systemically and within the lungs.[7,8,51-53] Crucially, we show here for the first time that targeting the anaphylotoxin receptors C3aR and C5aR in nonimmune respiratory cells can prevent intrinsic lung inflammation and tissue damage. This opens up the exciting possibility that complement inhibitors can be applied in the treatment of ARDS in patients with severe COVID-19.

We thank our technicians Denise Grässle, Isolde Enz, and Ruth Mader, as well as Dr Paul Hörtnagl, Central Institute for Blood Transfusion & Immunological Department, and Dr Manfred Nairz, University Clinics for Internal Medicine II, for their valuable help and support regarding this manuscript. The research reagents for SARS-CoV-2 RNA (National Institute for Biological Standards and Control 19/304) were obtained from the National Institute for Biological Standards and Control, UK. SARS-related coronavirus 2, Isolate Italy-INMI1 (# NR-52284) was deposited by Dr Maria R. Capobianchi for distribution through BEI Resources, National Institute of Allergy and Infectious Diseases (NIAID), National Institutes of Health (NIH). SARS-related coronavirus 2, Isolate USA-WA1/2020 (# NR-52281) was deposited by the Centers for Disease Control and Prevention and obtained through BEI Resources, NIAID, NIH. SARS-related coronavirus 2, Isolate Hong Kong/VM20001061/2020 (# NR-52282) was obtained through BEI Resources, NIAID, NIH.

Key messages

- **SARS-CoV-2 exposure leads to extensive intracellular C3 activation in primary respiratory cells.**
- **Extensive intracellular C3 activation is associated with massive destruction of the epithelial barrier, anaphylatoxin, and proinflammatory cytokine production from nonimmune airway epithelia.**
- **SARS-CoV-2–mediated, destructive effects at epithelial barrier sides can be reversed in particular by blocking anaphylatoxin receptor C5aR2.**

REFERENCES

1. Magro G. COVID-19: review on latest available drugs and therapies against SARS-CoV-2. Coagulation and inflammation cross-talking. Virus Res 2020;286:198070.
2. Zhu N, Zhang D, Wang W, Li X, Yang B, Song J, et al. A novel coronavirus from patients with pneumonia in China, 2019. N Engl J Med 2020;382:727-33.
3. Tang N, Li D, Wang X, Sun Z. Abnormal coagulation parameters are associated with poor prognosis in patients with novel coronavirus pneumonia. J Thromb Haemost 2020;18:844-7.
4. Wang D, Hu B, Hu C, Zhu F, Liu X, Zhang J, et al. Clinical characteristics of 138 hospitalized patients with 2019 novel coronavirus-infected pneumonia in Wuhan, China. JAMA 2020;323:1061-9.
5. Chen G, Wu D, Guo W, Cao Y, Huang D, Wang H, et al. Clinical and immunologic features in severe and moderate coronavirus disease 2019. J Clin Invest 2020;130:2620-9.
6. Huang C, Wang Y, Li X, Ren L, Zhao J, Hu Y, et al. Clinical features of patients infected with 2019 novel coronavirus in Wuhan, China. Lancet 2020;395:497-506.
7. Jodele S, Kohl J. Tackling COVID-19 infection through complement-targeted immunotherapy [published online ahead of print July 9, 2020]. Br J Pharmacol. https://doi.org/10.1111/bph.15187.
8. Yan B, Freiwald T, Chauss D, Wang L, West E, Bibby J, et al. SARS-CoV2 drives JAK1/2-dependent local and systemic complement hyper-activation [published online ahead of print June 9, 2020]. Res Sq. https://doi.org/10.21203/rs.3.rs-33390/v1.
9. Ramlall V, Thangaraj PM, Meydan C, Foox J, Butler D, Kim J, et al. Immune complement and coagulation dysfunction in adverse outcomes of SARS-CoV-2 infection. Nat Med 2020;26:1609-15.
10. Zaderer V, Hermann M, Lass-Florl C, Posch W, Wilflingseder D. Turning the world upside-down in cellulose for improved culturing and imaging of respiratory challenges within a human 3D model. Cells 2019;8:1292.
11. Chandorkar P, Posch W, Zaderer V, Blatzer M, Steger M, Ammann CG, et al. Fast-track development of an in vitro 3D lung/immune cell model to study Aspergillus infections. Sci Rep 2017;7:11644.
12. Sachs N, Papaspyropoulos A, Zomer-van Ommen DD, Heo I, Bottinger L, Klay D, et al. Long-term expanding human airway organoids for disease modeling. EMBO J 2019;38:e100300.
13. Dijkstra KK, Monkhorst K, Schipper LJ, Hartemink KJ, Smit EF, Kaing S, et al. Challenges in establishing pure lung cancer organoids limit their utility for personalized medicine. Cell Rep 2020;31:107588.
14. Gamage AM, Tan KS, Chan WOY, Liu J, Tan CW, Ong YK, et al. Infection of human nasal epithelial cells with SARS-CoV-2 and a 382-nt deletion isolate lacking ORF8 reveals similar viral kinetics and host transcriptional profiles. PLoS Pathog 2020;16:e1009130.
15. Zhou J, Li C, Sachs N, Chiu MC, Wong BH, Chu H, et al. Differentiated human airway organoids to assess infectivity of emerging influenza virus. Proc Natl Acad Sci U S A 2018;115:6822-7.
16. Matsuyama S, Nao N, Shirato K, Kawase M, Saito S, Takayama I, et al. Enhanced isolation of SARS-CoV-2 by TMPRSS2-expressing cells. Proc Natl Acad Sci U S A 2020;117:7001-3.
17. Mollnes TE, Lea T, Harboe M, Tschopp J. Monoclonal antibodies recognizing a neoantigen of poly(C9) detect the human terminal complement complex in tissue and plasma. Scand J Immunol 1985;22:183-95.
18. Zhu N, Wang W, Liu Z, Liang C, Wang W, Ye F, et al. Morphogenesis and cytopathic effect of SARS-CoV-2 infection in human airway epithelial cells. Nat Commun 2020;11:3910.
19. Dijkman R, Jebbink MF, Koekkoek SM, Deijs M, Jonsdottir HR, Molenkamp R, et al. Isolation and characterization of current human coronavirus strains in primary human epithelial cell cultures reveal differences in target cell tropism. J Virol 2013;87:6081-90.
20. Sims AC, Burkett SE, Yount B, Pickles RJ. SARS-CoV replication and pathogenesis in an in vitro model of the human conducting airway epithelium. Virus Res 2008;133:33-44.
21. Sowinski S, Jolly C, Berninghausen O, Purbhoo MA, Chauveau A, Köhler K, et al. Membrane nanotubes physically connect T cells over long distances presenting a novel route for HIV-1 transmission. Nature Cell Biol 2008;10:211-9.
22. Buchrieser J, Dufloo J, Hubert M, Monel B, Planas D, Rajah MM, et al. Syncytia formation by SARS-CoV-2-infected cells. EMBO J 2020;39:e106267.
23. Bussani R, Schneider E, Zentilin L, Collesi C, Ali H, Braga L, et al. Persistence of viral RNA, pneumocyte syncytia and thrombosis are hallmarks of advanced COVID-19 pathology. EBioMedicine 2020;61:103104.
24. Gu H, Fisher AJ, Mickler EA, Duerson F III, Cummings OW, Peters-Golden M, et al. Contribution of the anaphylatoxin receptors, C3aR and C5aR, to the pathogenesis of pulmonary fibrosis. FASEB J 2016;30:2336-50.
25. Carvelli J, Demaria O, Vely F, Batista L, Benmansour NC, Fares J, et al. Association of COVID-19 inflammation with activation of the C5a-C5aR1 axis. Nature 2020;588:146-50.
26. Stoermer KA, Morrison TE. Complement and viral pathogenesis. Virology 2011;411:362-73.

27. Zhou F, Yu T, Du R, Fan G, Liu Y, Liu Z, et al. Clinical course and risk factors for mortality of adult inpatients with COVID-19 in Wuhan, China: a retrospective cohort study. Lancet 2020;395:1054-62.
28. Gu HM, Mickler EA, Cummings OW, Sandusky GE, Weber DJ, Gracon A, et al. Crosstalk between TGF-beta 1 and complement activation augments epithelial injury in pulmonary fibrosis. FASEB J 2014;28:4223-34.
29. Gralinski LE, Sheahan TP, Morrison TE, Menachery VD, Jensen K, Leist SR, et al. Complement activation contributes to severe acute respiratory syndrome coronavirus pathogenesis. mBio 2018;9:e01753-18.
30. Hiemstra PS. Parallel activities and interactions between antimicrobial peptides and complement in host defense at the airway epithelial surface. Mol Immunol 2015;68:28-30.
31. Yang Y, Shen C, Li J, Yuan J, Wei J, Huang F, et al. Plasma IP-10 and MCP-3 levels are highly associated with disease severity and predict the progression of COVID-19. J Allergy Clin Immunol 2020;146:119-27.e4.
32. D'Elia RV, Harrison K, Oyston PC, Lukaszewski RA, Clark GC. Targeting the "cytokine storm" for therapeutic benefit. Clin Vaccine Immunol 2013;20:319-27.
33. Laumonnier Y, Karsten CM, Kohl J. Novel insights into the expression pattern of anaphylatoxin receptors in mice and men. Mol Immunol 2017;89:44-58.
34. Schindler R, Gelfand JA, Dinarello CA. Recombinant C5a stimulates transcription rather than translation of interleukin-1 (IL-1) and tumor necrosis factor: translational signal provided by lipopolysaccharide or IL-1 itself. Blood 1990; 76:1631-8.
35. Sun L, Guo RF, Gao H, Sarma JV, Zetoune FS, Ward PA. Attenuation of IgG immune complex-induced acute lung injury by silencing C5aR in lung epithelial cells. FASEB J 2009;23:3808-18.
36. Robbins RA, Russ WD, Rasmussen JK, Clayton MM. Activation of the complement system in the adult respiratory distress syndrome. Am Rev Respir Dis 1987;135:651-8.
37. Arbore G, West EE, Spolski R, Robertson AAB, Klos A, Rheinheimer C, et al. T helper 1 immunity requires complement-driven NLRP3 inflammasome activity in CD4(+) T cells. Science 2016;352:aad1210.
38. Arbore G, Kemper C, Kolev M. Intracellular complement—the complosome—in immune cell regulation. Mol Immunol 2017;89:2-9.
39. Hackett NR, Butler MW, Shaykhiev R, Salit J, Omberg L, Rodriguez-Flores JL, et al. RNA-Seq quantification of the human small airway epithelium transcriptome. BMC Genomics 2012;13:82.
40. Drouin SM, Kildsgaard J, Haviland J, Zabner J, Jia HP, McCray PB Jr, et al. Expression of the complement anaphylatoxin C3a and C5a receptors on bronchial epithelial and smooth muscle cells in models of sepsis and asthma. J Immunol 2001;166:2025-32.
41. Kulkarni HS, Liszewski MK, Brody SL, Atkinson JP. The complement system in the airway epithelium: an overlooked host defense mechanism and therapeutic target? J Allergy Clin Immunol 2018;141:1582-6.e1.
42. Kalant D, Cain SA, Maslowska M, Sniderman AD, Cianflone K, Monk PN. The chemoattractant receptor-like protein C5L2 binds the C3a des-Arg77/acylation-stimulating protein. J Biol Chem 2003;278:11123-9.
43. Kalant D, MacLaren R, Cui W, Samanta R, Monk PN, Laporte SA, et al. C5L2 is a functional receptor for acylation-stimulating protein. J Biol Chem 2005;280: 23936-44.
44. Cui W, Lapointe M, Gauvreau D, Kalant D, Cianflone K. Recombinant C3adesArg/acylation stimulating protein (ASP) is highly bioactive: a critical evaluation of C5L2 binding and 3T3-L1 adipocyte activation. Mol Immunol 2009;46:3207-17.
45. Zhang T, Garstka MA, Li K. The controversial C5a receptor C5aR2: its role in health and disease. J Immunol Res 2017;2017:8193932.
46. Li XX, Lee JD, Kemper C, Woodruff TM. The complement receptor C5aR2: a powerful modulator of innate and adaptive immunity. J Immunol 2019;202:3339-48.
47. Yamamoto H, Fara A, Chandra A, Cardone J, Dasgupta P, Kemper C. Role of complement in modulation of TH2 response in prostate cancer cells. Immunobiology 2012;217:1200.
48. Mastaglio S, Ruggeri A, Risitano AM, Angelillo P, Yancopoulou D, Mastellos DC, et al. The first case of COVID-19 treated with the complement C3 inhibitor AMY-101. Clin Immunol 2020;215:108450.
49. Diurno F, Numis FG, Porta G, Cirillo F, Maddaluno S, Ragozzino A, et al. Eculizumab treatment in patients with COVID-19: preliminary results from real life ASL Napoli 2 Nord experience. Eur Rev Med Pharmacol Sci 2020;24: 4040-7.
50. Mastellos DC, Ricklin D, Lambris JD. Clinical promise of next-generation complement therapeutics. Nat Rev Drug Discov 2019;18:707-29.
51. Gao T, Hu M, Zhang X, Li H, Zhu L, Liu H, et al. Highly pathogenic coronavirus N protein aggravates lung injury by MASP-2-mediated complement over-activation. medRxiv 20202020.03.29.20041962.
52. Lipworth B, Chan R, Lipworth S, RuiWen Kuo C. Weathering the cytokine storm in susceptible patients with severe SARS-CoV-2 infection. J Allergy Clin Immunol Pract 2020;8:1798-801.
53. Magro C, Mulvey JJ, Berlin D, Nuovo G, Salvatore S, Harp J, et al. Complement associated microvascular injury and thrombosis in the pathogenesis of severe COVID-19 infection: a report of five cases. Transl Res 2020;220:1-13.

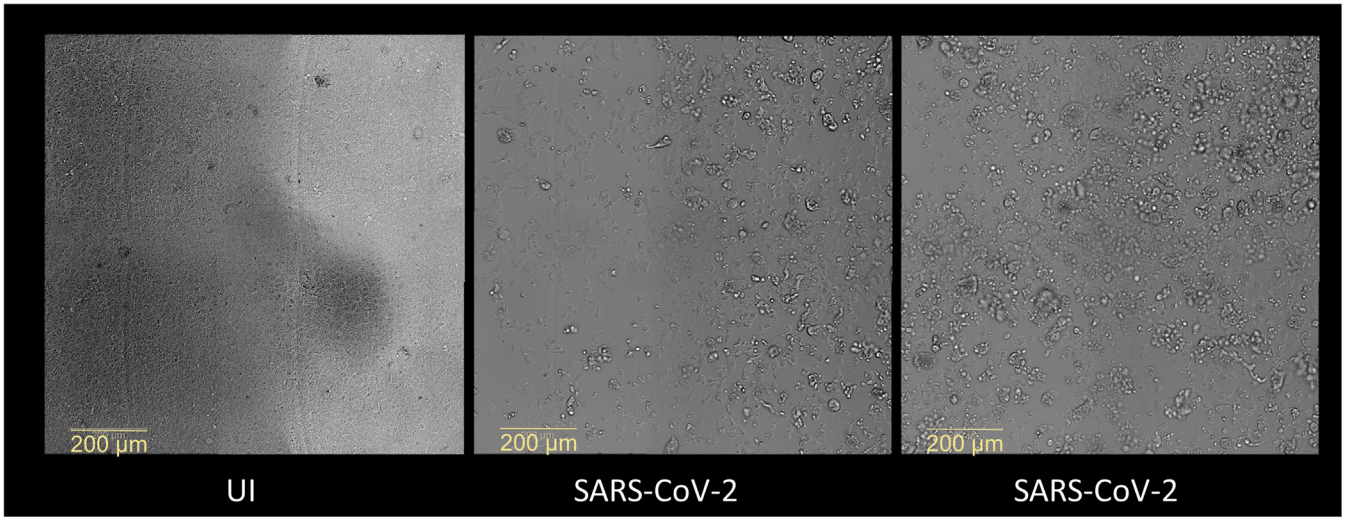

FIG E1. SARS-CoV-2 infection induces CPEs and reduces monolayer integrity in Vero/TMPRSS2 cells. Vero/TMPRSS2 were either left untreated (left image) or infected with SARS-CoV-2 derived from clinical isolates (middle and right images). Two days postinfection, cells were visualized using BF microscopy. Representative images of 3 independent experiments are shown. *BF*, Brightfield.

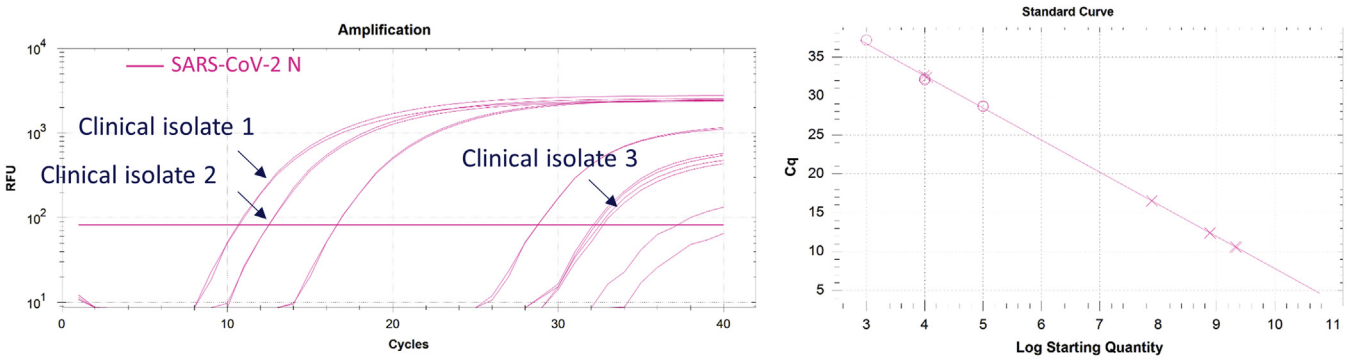

Sample	Cq Mean	Log Starting Quantity (SQ) Mean
Clinical isolate 1	8.19	11.964
Clinical isolate 2	11.99	10.318
Clinical isolate 3	32.42	3.497

Sample	TCID50 Dilution Factor	TCID50 RNA copies
Clinical isolate 1	$1/10^{11}$	10
Clinical isolate 2	$1/10^{10}$	10
Clinical isolate 3	$1/10^{3}$	10

FIG E2. Determination of TCID50 of clinical SARS-CoV-2 isolates used in this study. The absolute levels of viral RNA derived from clinical specimens and then subsequently propagated in Vero/TMPRSS2 cells were quantified using real-time RT-PCR with SARS-CoV-2–specific primer/probe pairs for the nucleocapsid N1 and N2 regions. A representative PCR quantification from 3 different isolates using the N2 primer/probe set is illustrated on the left, with the standard curve shown on the right. Tables below depict log starting quantities and TCID50. Using these isolates, a TCID50 on Vero/TMPRSS2 cells was performed and copy numbers calculated to infect 50% of the tissue cultures. *TCID50*, Tissue culture infectious dose 50.

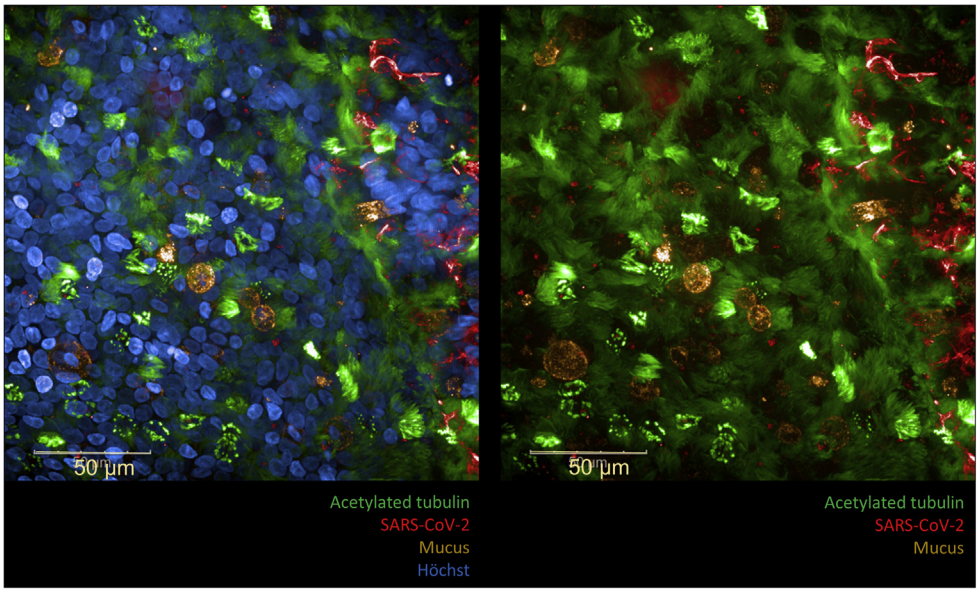

FIG E3. SARS-CoV-2 can infect both ciliated and mucus-producing cells in an HAE model. HAE cells were infected with SARS-CoV-2 at an MOI of 0.1. Cells (2 dpi) were fixed and stained for Hoechst (blue), SARS-CoV-2 S1/N (red), acetylated tubulin (green), and mucus-producing cells (orange) and then analyzed by confocal microscopy. On the left, a representative overview of HAE cells stained with Hoechst for nuclei (blue), acetylated tubulin (green), mucus-producing cells (orange), and virus (red) is depicted; on the right, the Hoechst channel was switched off to more clearly show viral distribution over the epithelium.

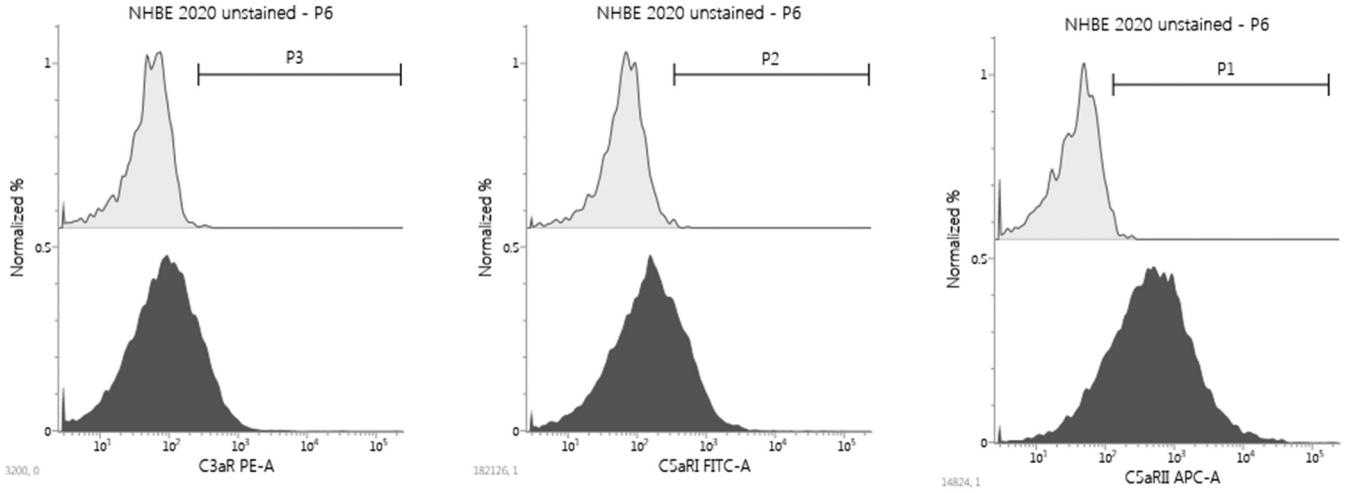

FIG E4. C5aR2 is the most abundantly expressed anaphylatoxin receptor on HAE monolayers. HAE monolayers were analyzed for their expression of C3aR, C5aR1, and C5aR2 by flow cytometry. Monolayers of HAE cells solely express higher levels of C5aR (dark gray) compared with isotype controls (light gray), whereas only low levels of C3aR and C5aR1 were analyzed. Experiments were repeated thrice independently.

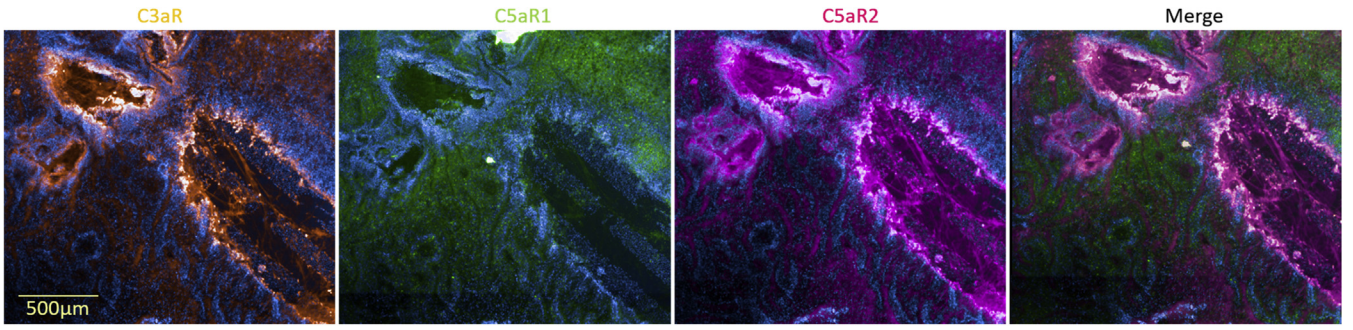

FIG E5. Anaphylatoxin receptors C3aR, C5aR1, and C5aR2 are expressed on HAE 3D tissue models. In contrast, all 3 receptors (C3aR, orange; C5aR1, green; C5aR2, pink) were illustrated by confocal microscopy on 3D tissue models. Experiments were repeated thrice independently.

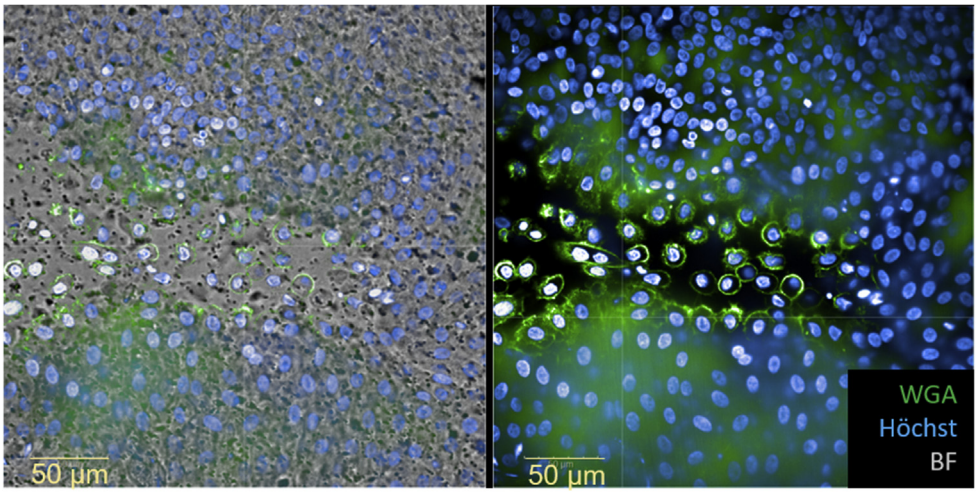

FIG E6. Recombinant C5a causes destruction of highly differentiated HAE. Addition of C5a (1 µg/mL) to highly differentiated HAE resulted in massive destruction of the tissue model in absence of SARS-CoV-2 infection. On the left, BF, Hoechst, and WGA and on the right, Hoechst and WGA are depicted. Multiple fields were analyzed, verifying the damage caused by addition of recombinant C5a. *BF*, Brightfield; *WGA*, wheat germ agglutinin.